Atmos. Meas. Tech. Discuss., 6, 1143–1199, 2013
www.atmos-meas-tech-discuss.net/6/1143/2013/
doi:10.5194/amtd-6-1143-2013

Atmospheric Measurement Techniques Discussions

Assessment of the CALIPSO Lidar 532 nm version 3 lidar ratio models using a ground-based lidar and AERONET sun photometers in Brazil

F. J. S. Lopes[1,2], **E. Landulfo**[2], **and M. A. Vaughan**[3]

[1]Institute of Astronomy, Geophysics and Atmospheric Sciences (IAG), University of São Paulo (USP), Sao Paulo, SP, Brazil
[2]Center for Lasers and Application – Nuclear and Energy Research Institute (IPEN/CNEN), Sao Paulo, SP, Brazil
[3]NASA Langley Research Center, Hampton, VA, USA

Received: 21 December 2012 – Accepted: 20 January 2013 – Published: 1 February 2013

Correspondence to: F. J. S. Lopes (fabiolopes@usp.br), E. Landulfo (elandulf@ipen.br)

Published by Copernicus Publications on behalf of the European Geosciences Union.

Abstract

Since the Cloud-Aerosol Lidar and Infrared Pathfinder Satellite Observations (CALIPSO) satellite first began probing the Earth's atmosphere on 13 June 2006, several research groups dedicated to investigating the atmosphere's optical properties have conducted measurement campaigns to validate the CALIPSO data products. Recently, in order to address the lack of CALIPSO validation studies in the Southern Hemisphere, and especially the South American continent, the Lasers Environmental Applications Research Group at Brazil's Nuclear and Energy Research Institute (IPEN) initiated efforts to assess CALIPSO's aerosol lidar ratio estimates using two ground-based remote sensing instruments: a single elastic backscatter lidar system and the AERONET sun photometers installed at five different locations in Brazil. In this study we develop a validation methodology to assess the accuracy of the modeled values of the lidar ratios used by the CALIPSO extinction algorithms. We recognize that the quality of any comparisons between satellite and ground-based measurements depends on the degree to which the instruments are collocated, and that even selecting the best spatial and temporal matches does not provide an unequivocal guarantee that both instruments are measuring the same air mass. The validation methodology presented in this study therefore applies backward and forward air mass trajectories in order to obtain the best possible match between the air masses sampled by the satellite and the ground-based instruments, and thus reduces the uncertainties associated with aerosol air mass variations. Quantitative comparisons of lidar ratio values determined from the combination of AERONET optical depth measurements and CALIOP integrated attenuated backscatter show good agreement with the model values assigned by the CALIOP algorithm. These comparisons yield a mean percentage difference of $-2\,\% \pm 26\,\%$. Similarly, lidar ratio values retrieved by the elastic backscatter lidar system at IPEN show a mean percentage difference of $-2\,\% \pm 15\,\%$ when compared with CALIOP's lidar ratio. These results confirm the accuracy in the lidar ratio estimates

AMTD
6, 1143–1199, 2013

provided by the CALIOP algorithms to within an uncertainty range of no more than 30 %.

1 Introduction

Aerosols and clouds play an important role in the Earth's radiation budget since their physical and optical properties affect the scattering and absorption processes of solar radiation (Solomon et al., 2007). Clouds act on atmospheric radiation processes by reflecting incoming sunlight back into space and by trapping thermal radiation emitted from the Earth's surface. Aerosols can act to either cool or warm the atmosphere. Cooling occurs when aerosols scatter incoming sun radiation back into space, whereas warming occurs due the absorption of the incoming sunlight. Moreover, aerosol particles can act as cloud condensation nuclei (CCN) affecting the concentration, size and lifetime of clouds (Anderson et al., 2003; Charlson et al., 1992). Aerosols affect climate processes on both local and global scales, thus representing a large source of uncertainties in the prediction of climate changes, mainly due their spatial and temporal variability (Anderson et al., 2005). Aerosol optical and physical properties are highly complex, and vary considerably due differences in their composition, distribution, sources (natural or anthropogenic) and local meteorology. One of the main challenges in the atmospheric sciences lies in acquiring more accurate knowledge about aerosol and cloud properties and how their interactions can affect climate model predictions. In the last decades, several remote sensing platforms – i.e. spaceborne, aircraft and ground-based measurement systems – were developed or improved to conduct studies of aerosol and cloud optical properties on local and global scales, as well as to provide the scientific basis for understanding the Earth's climate system. Most of our current understanding of aerosol influences in climate change processes has been developed from the study of horizontal distributions of aerosols derived from space-based passive remote sensor measurements (e.g. the Moderate Resolution Imaging Spectroradiometer MODIS). However, since 2006 the Cloud-Aerosol Lidar and Infrared

AMTD
6, 1143–1199, 2013

Pathfinder Satellite Observations (CALIPSO) satellite has retrieved vertical profiles of aerosols and clouds on a global scale, providing important contributions in atmospheric science studies and also complementing our knowledge of the horizontal distributions (Winker et al., 2009, 2010).

The CALIPSO mission is a partnership program developed by the United States' National Aeronautics and Space Administration (NASA) and the Centre National d'Etudes Spatiales (CNES) from France, and has as its principal purpose the retrieval of spatial and optical properties of aerosols and clouds in the vertical profile using the lidar (Light Detection and Ranging) technique. The CALIPSO satellite maintains a 705 km sun-synchronous polar orbit with a velocity of about 7 $km\,s^{-1}$ and the laser operates at a pulse repetition rate of 20.16 Hz (Hunt et al., 2009). The primary instrument aboard CALIPSO is the Cloud-Aerosol Lidar with Orthogonal Polarization (CALIOP). CALIOP is a two-wavelength elastic backscatter system, which implies an extra challenge in the retrieval of atmosphere optical properties, since its signals do not contain all of the information required to fully resolve the lidar equation, and therefore aerosol backscatter and extinction coefficients must be retrieved using assumed or modeled values of the so-called extinction-to-backscatter ratio (a.k.a. lidar ratio – LR) (Klett, 1985). For this reason, validation methodologies using ground-based instruments are needed to assess the accuracy of both the modeled and the retrieved optical properties reported in the CALIPSO data products.

Since the launch of CALIPSO, several validation studies have been conducted to assess CALIOP's algorithm performance and its data products. These validation studies used different methodologies and approaches, as well as different instruments, including both ground-based and airborne remote sensing systems. Kim et al. (2008) analyzed six cases comparing CALIOP measurements to coincident observations from a ground-based lidar in Seoul, Korea. Several other studies have been conducted comparing CALIOP data products to similar products produced using ground-based elastic backscattering systems (e.g. Tao et al., 2008a; Wu et al., 2011), or ground-based Raman lidar systems in the context of EARLINET (Mona et al., 2009; Mamouri

AMTD
6, 1143–1199, 2013

et al., 2009; Pappalardo et al., 2010). Ground-based sun photometer measurements (i.e. AERONET) have also been used in several recent assessments of CALIOP modeled lidar ratios and aerosol optical depths (Schuster et al., 2012; Omar et al., 2013). Other studies have compared CALIOP results to the data products from other satellites. Weisz et al. (2007) used cloud-data products from the Atmospheric Infrared Sounder (AIRS) and MODIS to retrieve estimates of cloud top heights and compare with those obtained using the active sensors such as Cloud Profiling Radar (CPR) and the CALIOP, onboard the CloudSat and CALIPSO satellites, respectively. Kittaka et al. (2011) compared column aerosol optical depth (AOD) values retrieved by MODIS and CALIOP at 532 nm, showing there is acceptable agreement between the two sensors in ocean regions with low cloudiness, and some differences in the AOD overland. The same study indicated that changes in the selection of the lidar ratio values used in the CALIOP aerosol retrieval would be sufficient to provide a regional mean AOD consistent with that retrieved from MODIS. Some other validation studies used different types of lidar systems onboard aircraft flying in the same trajectory as the CALIPSO satellite. For instance, McGill et al. (2007) qualitatively compared the vertical distribution of clouds measured by CALIOP and the Cloud Physics Lidar (CPL) system onboard NASA's high-altitude ER2 aircraft. Subsequent studies using CPL data by Yorks et al. (2011) and Hlavka et al. (2012) provide quantitative assessments of, respectively, the CALIOP layer detection scheme and the accuracy of the CALIOP cirrus cloud extinction retrievals.

Numerous validation studies have been carried out using the NASA Langley Research Center (LaRC) High Spectral Resolution Lidar (HSRL) deployed onboard the Langley B-200 aircraft flying in the same trajectory as the CALIPSO satellite (Burton et al., 2010; McPherson et al., 2010). Kacenelenbogen et al. (2011) presented a case study using measurements from several instruments, including the LaRC HSRL, the AERONET sun photometers, MODIS, and the POLarization and Directionality of Earth's Reflectances (POLDER) satellite, to compare multiple AOD values with those retrieved by CALIOP. This study suggests that CALIOP consistently underestimates the

AMTD
6, 1143–1199, 2013

MODIS AOD values, and investigates possible causes, including CALIOP's low signal-to-noise ratio, cloud contamination, and potentially erroneous values of the aerosol extinction-to-backscatter ratio provided by the CALIOP aerosol models. The most extensive study of CALIOP 532 nm calibration was carried out by Rogers et al. (2011) in a quantitative assessment using LaRC HSRL measurements over and near the North American continent. Comparisons of the 532 nm total attenuated backscatter signal retrieved by both systems showed agreement to within 2.7 % ± 2.1 % and 2.9 % ± 3.9 % (CALIOP lower) during nighttime and daytime, respectively, indicating the accuracy of the CALIOP 532 nm calibration algorithms.

The vast majority of the ground-based and airborne validation studies have been conducted in the North Hemisphere. To our knowledge, the sole exceptions to date are the global AERONET studies conducted by Schuster et al. (2012) and Omar et al. (2013). There is a distinct lack of CALIOP validation studies in the South Hemisphere, and this is especially notable in the South America territory, which is a region directly affected by the South Atlantic Anomaly (SAA) (Hunt et al., 2009; Powell et al., 2009). The SAA radiation effects can introduce large errors in the CALIOP calibration procedure, which in turn can lead to misclassification or a failure to detect aerosol layers. The validation methodology developed in this paper is, to the best of our knowledge, the first validation study focused on the CALIOP products reported over South America. In order to assess the accuracy and performance of the CALIOP algorithms, two types of ground-based instruments were used: the AERONET sun photometers installed at five different locations in the Brazilian territory, and an elastic backscatter lidar in the city of São Paulo. The coincidence of the measurements between the CALIPSO satellite and the ground-based systems was determined by taking into account both physical and atmospheric conditions. In addition, the LR values retrieved by the ground-based lidar system were compared with those assigned by the CALIOP algorithm. AERONET AOD products were used to derive the most likely LR values, and these too were compared with the values assigned by the CALIOP algorithms. The main objective of this study is to present the first quantitative results of the mean bias of the lidar ratio values of

AMTD
6, 1143–1199, 2013

the CALIOP algorithms and the ground-based systems. This first validation of CALIOP data products reported in the South America region is divided as follows. Section 2 describes the three sensors and their respective data products; i.e. a ground-based elastic backscatter lidar system, the AERONET sun photometers, and the CALIOP system aboard the CALIPSO satellite. The validation methodology is presented in the Sect. 3. In this section we also present the family of algorithms created for the validation analysis, and enumerate the necessary conditions for obtaining valid comparisons between the data from the three systems. Comparisons of assigned, derived, and measured quantities are presented in Sect. 4 and then discussed in the context of other validation studies in Sect. 5.

2 Instruments

This study assesses the performance of the CALIOP aerosol optical properties retrieval. We focus mainly on the lidar ratio values assigned by the CALIOP algorithms, using a dataset derived from the AERONET photometers and the elastic backscatter lidar system operated by IPEN. In this section we present the relevant details of each of the three instruments.

2.1 AERONET Sun photometer

The AErosol RObotic NETwork (AERONET) (Holben et al., 1998) is an international federation of ground-based sun photometers which provide automatic sun and sky scanning measurements. Using direct sun measurements, AERONET provides both AOD and the Ångström exponent (å), which gives the wavelength dependence of the AOD. By using multiangular and multispectral measurements of atmospheric radiances and applying a flexible inversion algorithm (Dubovik and King, 2000), the AERONET data can also provide several additional aerosol optical parameters, such as size distributions, single scattering albedo and refractive index. The operating principle of this

AMTD
6, 1143–1199, 2013

system is to acquire aureole and sky radiance observations using a large number of solar scattering angles through a constant aerosol profile, and thus retrieve the aerosol size distribution, the phase function and the AOD. The channels used are centered at 340, 440, 500, 670, 870, 940 and 1020 nm, with a 1.2° full angle FOV. The measurements are taken by pointing the instrument directly at the sun, or elsewhere in the sky in nine standard angular intervals employed uniformly by the AERONET network (Holben et al., 1998). The sun photometer is calibrated periodically, either by a remote computer or locally under the supervision of the AERONET network. The calibration methodology assures a coefficient error less than 5 %; nonetheless, instrumental variations, calibration, atmospheric, and methodological factors can influence the precision and accuracy of the derived optical thickness, and effectively the total uncertainty in the AERONET AOD is about 10 % (Dubovik et al., 2000). The inversion of the solar radiances to retrieve AOD values is based on the Beer-Lambert-Bouguer law, given by Eq. (1), assuming that the contribution of multiple scattering within the field of view of the photometer is negligible.

$$I_\lambda = I_{0,\lambda} \exp\left[-\frac{\tau_\lambda}{\mu_s}\right] \quad (1)$$

I_λ and $I_{0,\lambda}$, are the solar irradiances at the top of the atmosphere and at ground level, respectively, and μ_s is the cosine of the solar zenith angle. τ_λ is the path-integrated atmospheric optical depth due to the molecular (Rayleigh) (τ_λ^m) and aerosol (τ_λ^{aer}) scattering, as well the ozone and water vapor absorptions at 670 nm and 870 nm (τ_λ^g). The aerosol optical depth at 532 nm is retrieved using Eq. (2), derived from the spectral dependence of the aerosol optical depth in the visible spectrum (Ångström, 1964):

$$\tau_{532}^{aer} = \tau_{500}^{aer}\left[\frac{532}{500}\right]^{-å}. \quad (2)$$

AMTD
6, 1143–1199, 2013

The Ångström exponent å is derived from the measured optical thickness in the blue (440 nm) and red channels (675 nm):

$$\text{å} = -\frac{\log\left[\frac{\tau_{440}^{\text{aer}}}{\tau_{675}^{\text{aer}}}\right]}{\log\left[\frac{440}{675}\right]} \tag{3}$$

The AERONET AOD values, together with the layer integrated attenuated backscatter coefficient retrieved from CALIOP, will be employed to obtain the most likely lidar ratio values, which will then be compared with those assigned by the CALIOP aerosol subtyping scheme (Omar et al., 2009). Moreover, using the single-scattering albedo ($\omega(\lambda)$) and 180° phase function values (P(180°)) retrieved from the AERONET inversion algorithm, the backscatter-to-extinction ratio shown in Eq. (4) can be calculated and compared with the values assigned by the CALIOP algorithms.

$$S_{\text{aer}} = \frac{4\pi}{\omega(\lambda)P(180^{\circ})} \tag{4}$$

2.2 MSP-lidar system

The MSP-Lidar (Municipio de São Paulo-Lidar) is a single-wavelength, zenith-pointing elastic backscatter system operating in a coaxial mode (Landulfo et al., 2003). The light source is a frequency doubled commercial Nd:YAG laser (Brilliant, Quantel SA) that emits 532 nm pulses at a fixed repetition rate of 20 Hz. The laser can be configured to generate average emitted powers of up to 3.3 W, and has a beam divergence of less than 0.5 mrad. A 30 cm diameter telescope (focal length f = 1.3 m) is used to collect the backscattered laser light, which is then sent to a photomultiplier tube (PMT) coupled to a narrowband (1 nm FWHM) interference filter that reduces solar background during daytime operations and improves the signal-to-noise ratio (SNR). The PMT output signal is recorded by a transient recorder in both analog and photon-counting modes

AMTD
6, 1143–1199, 2013

(Landulfo et al., 2005). The telescope field of view (FOV) can be varied over a (0.5–5 mrad) range by using a small diaphragm. The lidar currently operates with a fixed FOV on the order of 1 mrad, which ensures full overlap between the telescope FOV and the laser beam at heights higher than 300 m above the lidar system. Once overlap is achieved, the system can probe the full extent of the troposphere (12–15 km).

2.2.1 Backscatter profile and lidar ratio retrieval

Retrieving the optical properties of the atmosphere from elastic backscatter lidar measurements requires the solution of Eq. (5):

$$P(\lambda,z) = \left(\frac{P_0 C_\lambda}{z^2}\right)\left[\beta_{\mathrm{m}}(\lambda,z)+\beta_{\mathrm{aer}}(\lambda,z)\right]\exp\left[-2\int_o^z \alpha_{\mathrm{m}}(\lambda,z')\mathrm{d}z'\right]\exp\left[-2\int_o^z \alpha_{\mathrm{aer}}(\lambda,z')\mathrm{d}z'\right] \quad (5)$$

In this expression

- $P(\lambda,z)$ is the lidar signal received from a distance z at the wavelength λ;
- P_0 is the emitted laser power;
- C_λ is the system calibration coefficient;
- $\alpha_{\mathrm{m}}(\lambda,z)$ is the molecular volume extinction coefficient at altitude z, which is related to the molecular two-way transmittance between the lidar and the range z; i.e.

$$T^2_{\mathrm{m}}(z) = \exp\left[-2\int_o^z \alpha_{\mathrm{m}}(\lambda,z')\mathrm{d}z'\right];$$

AMTD
6, 1143–1199, 2013

– $\alpha_{aer}(\lambda, z)$ is the volume extinction coefficient due the particulate loading at altitude z, and is related to the particulate two-way transmittance between the lidar and the range z; i.e.

$$T^2_{aer}(z) = \exp\left[-2\int_o^z \alpha_{aer}(\lambda, z')\mathrm{d}z'\right].$$

– $\beta_m(\lambda, z)$ and $\beta_{aer}(\lambda, z)$ are, respectively, the volume backscatter coefficients for molecules and particulates at range z.

In this work the particulate transmittance term can be rewritten according to the aerosol optical depth measured by the AERONET sun photometer:

$$T^2_{aer}(z) = \exp\left[-2S_{aer}\int_o^z \beta_{aer}(\lambda, z')\mathrm{d}z'\right] = \exp\left[-2\mathrm{AOD}_{\mathrm{AERONET}}\right]. \quad (6)$$

In the absence of additional measurements (e.g. as are acquired by Raman and HSRL systems), solving the lidar equation requires establishing a relation between $\alpha_{aer}(\lambda, z)$ and $\beta_{aer}(\lambda, z)$. This is typically achieved by assuming that the aerosol extinction-to-backscatter ratio is independent of altitude; i.e. that

$$S_{aer}(\lambda) = \frac{\alpha_{aer}(\lambda, z)}{\beta_{aer}(\lambda, z)} \quad (7)$$

However, it is known that the lidar ratio depends on several physical and chemical parameters of the aerosol being measured, such as refractive index and the size and shape distributions of the aerosol particles (Ackermann et al., 1998; Liou et al., 2002; Barnaba and Gobbi, 2002). For this reason, using an elastic backscatter system is a challenging task and a good knowledge of aerosol types and their associated

AMTD
6, 1143–1199, 2013

lidar ratios is essential for retrieving aerosol backscatter and extinction coefficient profiles, both for ground-based and satellite systems (Cattrall et al., 2005; Giannakaki et al., 2010). To solve the ill-posed problem of the lidar equation and obtain accurate backscatter and extinction coefficient profiles, we apply Klett's inversion method (Klett, 1981, 1985) to the MSP-Lidar measurements. The solutions are constrained using AOD values retrieved by the AERONET sun photometer installed about 400 m from the MSP-Lidar. By substituting Eq. (7) into Eq. (5), the lidar ratio and the extinction profile can be retrieved using an iterative technique similar to the CALIPSO algorithm for constrained solutions (Young and Vaughan, 2009) wherein the following pair of equations is simultaneously satisfied:

$$\beta_{\mathrm{aer}}(\lambda,z)+\beta_{\mathrm{m}}(\lambda,z)=\frac{z^2\left[P(\lambda,z)-P_0\right]\exp\left[-2(S_{\mathrm{aer}}-S_{\mathrm{m}})\int_o^z\beta_{\mathrm{m}}(\lambda,z')\mathrm{d}z'\right]}{1-2S_{\mathrm{aer}}\left[\int_o^z z'^2[P(\lambda,z')-P_0]\exp\left[-2(S_{\mathrm{aer}}-S_{\mathrm{m}})\int_o^{z'}\beta_{\mathrm{m}}(\lambda,z'')\mathrm{d}z''\right]\mathrm{d}z'\right]},$$

$$S_{\mathrm{aer}}\int_0^{\text{Aerosol Top Altitude}}\beta_{\mathrm{aer}}(\lambda,z')\mathrm{d}z'=\mathrm{AOD} \quad (8)$$

S_{m} is the molecular lidar ratio, and is discussed further below.

2.2.2 Calibration procedure

The calibration constant for the MSP-Lidar signal is determined by normalizing the backscatter signal at some reference clear altitude to a model molecular profile constructed using atmospheric temperature and pressure data measured by radiosondes.

AMTD
6, 1143–1199, 2013

This procedure uses the following equation:

$$C = \frac{\left[P(\lambda, z_{\text{ref}}) - P_0\right] z^2}{\beta_{\text{m}}(\lambda, z_{\text{ref}}) \exp\left[-2\int_{z_{\text{ref1}}}^{z_{\text{ref2}}} \alpha_{\text{m}}(\lambda, z)\text{d}z\right]} \quad (9)$$

The mean calibration constant is computed by averaging over a reference region considered to be clear of aerosols, typically between 8 km to 12 km. The molecular backscatter coefficients, $\beta_{\text{m}}(\lambda, z_{\text{ref}})$, are calculated based on the Bucholtz's approach (Bucholtz, 1995), following Eq. (10):

$$\beta_{\text{m}}(\lambda, z_{\text{ref}}) = N_{\text{s}} \sigma_{\text{Rayleigh}}(\lambda) \frac{P}{P_{\text{s}}} \frac{T_{\text{s}}}{T} \quad (10)$$

Here $\sigma_{\text{Rayleigh}}(\lambda)$ is the Rayleigh scattering cross section (Bucholtz, 1995), N_{s} is the molecular number density for standard air, and P and T are, respectively, the pressure and temperature measured by daily radiosonde launches from within São Paulo. The two-way transmittance term for molecules, $\exp\left[-2\int_{z_{\text{ref1}}}^{z_{\text{ref2}}} \alpha_{\text{m}}(\lambda, z)\text{d}z\right]$ is calculated using the relation $\alpha_{\text{m}}(\lambda, z_{\text{ref}}) = \beta_{\text{m}}(\lambda, z_{\text{ref}}) S_{\text{m}}$, where $\beta_{\text{m}}(\lambda, z_{\text{ref}})$ is the atmospheric volume backscatter coefficients for the molecular contributions in the reference range. $S_{\text{m}} = \frac{8\pi}{3}\kappa$, is the molecular extinction-to-backscatter ratio (molecular lidar ratio), and κ defines the dispersion of the refractive index and the King correction factor of air at 532 nm (Bucholtz, 1995; Bodhaine et al., 1999). In this work, the ozone contributions to the MSP-lidar signal will be considered negligible since the changes in the tropospheric ozone do not significantly affect the aerosol calculation (Mona et al., 2009).

2.3 CALIPSO satellite

CALIPSO satellite was launched in April 2006, and since then has been an integral part of NASA's A-Train satellite constellation (Stephens et al., 2002). CALIPSO

AMTD
6, 1143–1199, 2013

flies in a 705 km sun-synchronous polar orbit with an equator-crossing time of about 13:30 local solar time, covering the whole globe in a repeat cycle of 16 days (Winker et al., 2009). The CALIPSO payload consists of three co-aligned nadir-pointing instruments designed to operate autonomously and continuously. Two of these are passive sensors that provide a view of the atmosphere surrounding the lidar curtain, namely, a wide field-of-view camera (WFC) with a pixel spatial resolution of 125 m (Pitts et al., 2007), and a three-channel infrared imaging radiometer (IIR) with a spatial resolution of 1 km and a swath of 61 km (Garnier et al., 2012). The primary instrument is CALIOP, a two-wavelength (532 nm and 1064 nm), polarization-sensitive (at 532 nm) elastic backscatter lidar designed to provide global optical properties of aerosol and clouds. The CALIOP laser transmitter subsystem consists of two identical Nd:YAG lasers, each with a beam expander to reduce the divergence of the laser beam at the Earth's surface, and a beam steering system that ensures the alignment between the active transmitter and the receiver.

The lasers are diode-pumped and operate at a pulse repetition rate of 20.25 Hz. Each laser nominally generates a total of 220 mJ per pulse which is frequency-doubled to produce about 110 mJ of pulse energy at each of the two wavelengths (Hunt et al., 2009). The lasers are Q-switched to provide a pulse length of about 20 ns. The receiver subsystems measure the total attenuated backscatter signal intensity at 1064 nm and the two orthogonally polarized attenuated backscatter components at 532 nm. The CALIOP data products are assembled from the backscatter signals measured by the receiver system, and reported in two categories: level 1 products and level 2 products. Level 1 products are composed of calibrated and geolocated profiles of the attenuated backscatter signal, and are separated into three types: the total attenuated backscatter profile at 1064 nm, the total attenuated backscatter profile at 532 nm (i.e. the sum of parallel and perpendicular signals), and the perpendicular attenuated backscatter signal at 532 nm (Hostetler et al., 2006; Winker et al., 2009). The attenuated backscatter signal measured by the CALIOP system at the wavelength λ and range z can be written

AMTD
6, 1143–1199, 2013

as:

$$\beta'(\lambda,z) = \frac{z^2\left[P(z) - P_{\mathrm{bkg}}\right]}{C_\lambda E_\lambda G_\lambda} = \left[\beta_{\mathrm{m}}(\lambda,z) + \beta_{\mathrm{aer}}(\lambda,z)\right] T^2(z), \quad (11)$$

where $P(z)$ is the measured backscattered laser signal, P_{bkg} accounts for background signals and digitizer offset voltages, E_λ and G_λ are, respectively, the laser energy and electronic signal gain measured on-board the satellite, and C_λ is a calibration coefficient determined in post processing after the data has been downlinked to the ground station. $\beta_{\mathrm{aer}}(\lambda,z)$ and $\beta_{\mathrm{m}}(\lambda,z)$ are the aerosol and molecular backscatter coefficients, respectively, and $T^2(z)$ is the two-way transmittance due the aerosol and molecular scattering and ozone gas absorption from the CALIOP calibration region to range z, given as:

$$T^2(z_{\mathrm{c}},z) = \exp\left[-2\int \alpha(\lambda,z)\mathrm{d}z\right]. \quad (12)$$

In Eq. (12), the extinction coefficient $\alpha(\lambda,z)$ can be expanded in terms of the aerosol, molecular and ozone contributions; i.e. $\alpha(\lambda,z) = \alpha_{\mathrm{aer}}(\lambda,z) + \alpha_{\mathrm{m}}(\lambda,z) + \alpha_{\mathrm{O_3}}(\lambda,z)$, respectively. The quality and accuracy of the level 1 products, and therefore the level 2 products, depend on the accuracy of the calibration of the 532 nm parallel-channel. This calibration process normalizes the measured signal with respect to an atmospheric model (Russell et al., 1979; Powell et al., 2009) at high altitudes. The choice of the altitude range is critically important in order to obtain a backscatter signal with purely molecular contributions, while simultaneously ensuring sufficient signal-to-noise ratio (SNR) and maintaining a linear detector response. Through version 3 of the CALIPSO data products, the 532 nm parallel channel calibration coefficient has been consistently calculated in the altitude interval of 30–34 km, under the assumption that any stratospheric aerosol contributions are negligible (We note, however, that Vernier et al., 2009 have demonstrated that the stratospheric aerosol loading in this region can in fact be significant, leading to calibration errors that, depending on season and latitude, may

AMTD
6, 1143–1199, 2013

be as large as several percent). The calibration coefficients for the parallel channel measurements are computed according to Eq. (13), where the molecular and ozone contributions – i.e. $\beta_{532,\mathrm{m}}(z)$, $T^2_{532,\mathrm{m}}(z)$ and $T^2_{532,\mathrm{O_3}}$ – are derived from model temperature and pressure data provided by NASA Global Modeling and Assimilation Office (GMAO).

$$C_{532,\parallel} = \left[\frac{z^2}{E_{532}G_{532,\parallel}}\right]\left[\frac{P_{532,\parallel}(z) - P_{\mathrm{bkg},532,\parallel}(z)}{\beta_{532,\mathrm{m}}(z)T^2_{532,\mathrm{m}}(z)T^2_{532,\mathrm{O_3}}(z)}\right] \quad (13)$$

The molecular normalization technique described by Eq. (13) can only be applied to nighttime measurements. The CALIOP daytime measurements are affected by the high solar background, which dominates the pure molecular signal and drastically decreases the SNR in the nighttime calibration altitude range. Thus, in the daytime portion of the orbit, the calibration coefficients are derived by a piecewise linear interpolation scheme that is anchored by values derived from the adjacent nighttime portions of the orbit. Details of successive improvements in the CALIOP daytime calibration procedure are described in Hostetler et al. (2006) and Powell et al. (2008, 2009, 2010). The perpendicular channel is calibrated by inserting a pseudo-polarizer into the optical path of the 532 nm return signal, thus producing equal backscatter intensities in both channels and allowing the eletro-optical gain ratio between the two to be determined, as described by Hunt et al. (2009). Before starting the calibration procedure, the measured data are filtered in order to identify signal spikes resulting from high-energy protons or cosmic ray events. These extreme noise excursions are detected randomly throughout the orbits; however, they occur most frequently in the South Atlantic Anomaly region (SAA) (Hunt et al., 2009; Powell et al., 2009). The SSA occurs due the closest approach of the Van Allen radiation belts to the surface of the Earth. When the CALIPSO satellite overpasses the SAA region, the 532 nm photomultipliers can produce radiation-induced current spikes that are as much as two orders or magnitude larger than the pulses produced by single photoelectrons. Individual spikes

AMTD
6, 1143–1199, 2013

can adversely affect signal averages in low-signal regions, and multiple pulses can increase the dark noise level, with a corresponding decrease in the SNR (Hunt et al., 2009). The signal spikes from high-energy events can introduce large errors in the calibration procedure. To minimize the impacts of these spikes, a multi-step adaptive filtering procedure has been implemented to identify and remove signal outliers prior to processing, and thus ensure adequate SNR within the calibration procedure (Lee et al., 2008; Powell et al., 2009).

The level 2 products are derived from the level 1 products. Three different level 2 products are distributed: layer products, profile products and the vertical feature mask (VMF). Layer products provide the optical properties of aerosol and clouds integrated or averaged in each of the layers detected in the atmosphere. The profile products provide the retrieved backscatter and extinction profiles wherever layers are detected. The VFM provides a map of cloud and aerosol locations, and also their types. The level 2 products are generated by a sequence of inter-related algorithms that can be subdivided into three main modules. The first module, the Selective Iterative Boundary Locator (SYBIL), uses the level 1 attenuated backscatter profiles to identify cloud and aerosol layers (Vaughan et al., 2009). Once the layer boundaries are located, the cloud-aerosol discrimination (CAD) module uses the layer integrated attenuated backscatter coefficients, along with altitude and geophysical location to classify each layer as either aerosol or cloud (Liu et al., 2009). Aerosol layers are further classified into six different subtypes (Omar et al., 2009), while clouds are separated according to ice-water phase (Hu et al., 2009). Perhaps the most significant task performed by the aerosol subtyping algorithm is to associate each aerosol layer with a modeled lidar ratio that characterizes the assigned aerosol type. The CALIPSO aerosol models employed by this algorithm are based largely on a cluster analysis performed on a global AERONET dataset acquired between 1993 and 2002 (Omar et al., 2005).

According to the cluster analysis, six different types of aerosol were identified for use in the CALIOP retrieval scheme: dust, smoke, clean and polluted continental, polluted dust and clean marine. Each aerosol subtype is characterized by a lidar ratio

AMTD
6, 1143–1199, 2013

distribution (mean and standard deviation), as shown in Table 1. The lidar ratios initially determined by the cluster analysis for the dust and marine models were further refined using other measurements and methods (Omar et al., 2009). The aerosol typing and lidar ratio selection scheme uses derived level 1 products, such as the integrated attenuated backscatter at 532 nm and the integrated volume depolarization ratio (i.e. the ratio between the integrated perpendicular and parallel backscatter signals). These parameters are calculated by integrating the signal from the top to the base of each detected aerosol layer. However, these two parameters alone are not sufficient to determine the aerosol type, and thus the algorithm also uses geophysical information such as surface type (e.g. land vs. oceans, deserts vs. snow/tundra regions, etc.) and aerosol layer elevation, since lifting mechanisms can be very specific for different types of aerosol. All these physical and optical parameters are used as input in order to choose the most likely aerosol model and constrain the associated lidar ratio uncertainties (Omar et al., 2009). An accurate classification of the aerosol and cloud layers, and especially their LR values, is critically important for a successful retrieval of the aerosol and cloud optical properties that comprise the CALIOP level 2 data. An accurate classification of the aerosol and cloud layers found, and especially their LR values, is critically important for a successful retrieval of the aerosol and cloud optical properties which comprise the CALIOP level 2 data.

3 Validation methodology

To date, all CALIPSO validation studies using ground-based instruments have relied only on spatial and temporal correlations between CALIOP and the ground-based sensor(s) (Kim et al., 2008; Mamouri et al., 2009; Mona et al., 2009; Wu et al., 2011). However, this simple correlation does not unequivocally guarantee that both instruments are measuring the same air parcels. Even when one can obtain a statistically significant data set there will always be uncertainties associated with local variations of the aerosol air mass parcels. In order to reduce these uncertainties we use transport

AMTD
6, 1143–1199, 2013

model trajectories to identify the best possible match between the air masses sampled by CALIOP and the air masses sampled by the ground-based instruments. In this sense, the core of our validation methodology is to define "coincidence" not in terms of the proximity of measurements with respect to one another in time and/or space, but instead in terms of the proximity of the measurements with respect to a single air mass whose location may be spatially and temporally varying. We accomplish this by using transport models to generate backward or forward trajectories, as required, to ensure that the air/aerosol parcel measured at the validation site is, to the best of our ability, the same the air/aerosol parcel measured by the CALIPSO lidar. By requiring that the instruments probe the same air mass, rather than possibly different but nearby (in time and/or space) parcels, we expect to decrease the fundamental uncertainties introduced by spatial and temporal inhomogeneities.

The first step towards the development of our validation methodology was to decide the location (where) and time (when) to collect ground-based data correlated with CALIPSO satellite measurements. Within the Brazilian territory there are several AERONET sites strategically installed in areas that frequently experience large aerosol loadings. For this work we selected a measurement period from 2006 to 2009 for five operational AERONET locations: Rio Branco, Alta Floresta, Cuiabá, Campo Grande and São Paulo. Their geographical coordinates are given in Table 2 and their locations are presented in Fig. 1. These sites are located mainly in the North and Midwest regions of Brazil where the dominant vegetation types are savannah and rainforest. These native flora are now interspersed with numerous patches of pasture areas that are highly susceptible to fires during the so-called Brazilian dry season (May–October). These crop burning activities are responsible for the injection large amounts of biomass burning aerosols into the atmosphere (Artaxo et al., 2002). The presence of a characteristic type of aerosol loading in the atmosphere can help in the validation process. The São Paulo site, located in the Southeast region of Brazil, was chosen since it has two operational remote sensing systems, an AERONET sun photometer and the MSP-lidar. While these two sensors are situated within 400 m of each other, analysis of

AMTD
6, 1143–1199, 2013

measurements from the São Paulo site nevertheless faces challenges. Given the number of distinct aerosol sources within the city, combined with those brought by long- and mid-range regional transport, the São Paulo atmosphere is frequently filled by an amalgam of many different types of aerosols (Miranda and Andrade, 2005; Landulfo et al., 2008).

3.1 Conditions for coincident measures selection

According to Anderson et al. (2003), when comparing ground-based instruments and a spaceborne lidar, good correlations ($r > 0.9$) occur for time and space offsets less than 3 h and 60 km, and acceptable correlations ($r > 0.8$) occur for time and space offsets less than 6 h and 120 km. In a similar study comparing aerosol optical depths from MODIS and AERONET, Kovacs (2006) demonstrates that the correlation decreases by about 20 % for 200 km and 10 % for 140 km of distance. Thus, in order to match the CALIOP data with ground-based measurements in the Brazilian territory we used the following procedure based on the correlation results presented in the two previous sections. The COVERLAI (CALIPSO Overpass Locator Algorithm) was set up to select all days for which the CALIPSO satellite overflew the five ground sites within a horizontal range distance of $\Delta D \leq 100$ km. Subsequently, the MCSA (Multi-instrument Coincidence Selection Algorithm) selects all coincident measurements carried out by the ground-based systems, both AERONET and MSP-Lidar system, in a temporal matching window of up to 6 h, centered at the closest approach by CALIPSO. These two conditions are applied to minimize the uncertainties due the spatial and temporal in homogeneities in the atmospheric observation range. To ensure that all data were cloud-free, we relied on the number of layers detected, as reported in the CALIPSO 5-km Resolution Level 2 cloud layer products (Powell et al., 2011) using CLARA algorithm (Cloud-Aerosol Reader Algorithm). The CALIPSO level 2 5-km layer products present a set of spatial and optical properties (e.g. optical depth, layer base and top heights, etc.) for each individual feature detected within the vertical column of atmosphere. To select all coincident measurement days when both CALIOP and AERONET detected

AMTD
6, 1143–1199, 2013

cloud-free conditions at the time of the closest approach, the Number Layers Found (NLF) is analyzed. The NLF, which specifies the number of cloud layers detected for each 5-km resolution profile, was inspected for a spatial range of 100 km centered at the closest distance between CALIOP ground-track and the AERONET site (i.e. 20 consecutive 5-km profiles). Those cases for which the NLF was uniformly zero were flagged as cloud-free condition measurements. Since the objective of this study is to assess aerosol lidar ratios, all aerosol layers from the 5-km resolution aerosol layers products in spatial ranges flagged as cloud-free conditions were selected for analysis. We then inspected the cloud-aerosol discrimination (CAD) score for the selected aerosol layers. The CALIOP CAD algorithm discriminates between clouds and aerosols using probability distribution functions (PDFs) based on the differences in the optical and physical properties of aerosols and clouds (Liu et al., 2009). For this study we selected only those aerosol layers flagged with CAD scores between −50 and −100, where the larger the magnitude of the CAD score, the higher the confidence in the classification (Liu et al., 2009). This test ensures the selection of reliable aerosol layers. Once we have selected all cloud-free cases and identified all the aerosol 5-km resolution profiles with acceptable CAD score values, we used both the aerosol layer products and the aerosol profile products to calculate the so-called backscatter centroid. This quantity represents the altitude associated with the "backscatter center of mass" for each aerosol layer detected, and is computed using Eq. (14) (Vaughan et al., 2006), where x_i is the total attenuated backscatter signal at 532 nm at altitude Z_i:

$$C = \frac{\sum_{i=1}^{N} x_i Z_i}{\sum_{i=1}^{N} x_i} \tag{14}$$

The Level 2 aerosol layer products are used to determine layer top and bottom heights used in the centroid calculation. The backscatter centroids are employed as input data for the air mass trajectories subsequently computed using the HYSPLIT model (Draxler and Hess, 1998). Since the mesoscale variation and short lifetime of aerosols in the troposphere should be taken into account when comparing AOD measurements,

AMTD
6, 1143–1199, 2013

we use HYSPLIT trajectory modeling to investigate how the air mass parcels in the CALIPSO ground track region have moved with respect to the AERONET site. By using these trajectory models to better predict the motion of the air masses, we expect to improve the correlation between the optical properties (i.e. AOD and lidar ratio) measured by two different instruments separated spatially. Forward or backward trajectories and the appropriate model vertical velocity option are selected on a case-by-case basis. The starting time of the trajectories is set based on the time of the CALIPSO closest approach to the AERONET site, and the total trajectory run time is set to 6 h to guarantee at least acceptable air mass matching between CALIOP and the ground-based systems. Trajectories were initiated at the footprint latitude/longitude of the temporal midpoint of each 5-km CALIOP layer data. While the application of trajectory analysis decreases the available number of correlative measurements, it simultaneously strengthens the results retrieved from optical properties comparisons of both systems because it increases the likelihood of similar air parcels being probed by the ground instruments and CALIOP. Figure 2 shows the flowchart of the validation methodology algorithms, the data used as input and their output products.

3.2 Comparison of the optical properties – lidar ratio

After producing a merged data set satisfying all the imposed constraints, the layer integrated attenuated backscatter coefficient at 532 nm, γ'_{532}, is estimated for each of 20 consecutive 5-km horizontal resolution profiles for the selected validation days. Instead of using the estimates of γ'_{532} reported in the CALIPSO data products, we chose instead to calculate revised estimates of γ'_{532} using the equation derived by Platt (1973):

$$\gamma'_{\text{caliop}} = \frac{\left[1 - \exp(-2\eta\tau_{\text{caliop}})\right]}{2\eta S_{\text{caliop}}} \tag{15}$$

where η is a multiple scattering factor (η = 1 for CALIOP version 3 aerosol retrievals), and τ_{caliop} and S_{caliop} are, respectively, the 532 nm aerosol optical depth and the 532 nm

AMTD
6, 1143–1199, 2013

final lidar ratio reported in the CALIPSO level 2 aerosol layer products. We found in retrospect that our revised estimates of γ'_{caliop} showed reasonably good agreement with estimates of γ_{532} that are reported in the CALIPSO data product. A rearranged version of Eq. (15) will provide layer lidar ratio estimates for known values of optical depth and integrated attenuated backscatter, and will be used here to retrieve the "appropriate" values of S_{AC} (AERONET/CALIOP lidar ratio) using the AOD values retrieved from the AERONET sun photometers and the value of γ'_{caliop} at 532 nm given by the previous Eq. (15); i.e.

$$S_{\text{AC}} = \frac{\left[1 - \exp(-2\eta\tau_{\text{aeronet}})\right]}{2\eta\gamma'_{\text{caliop}}} \tag{16}$$

As described earlier, the AERONET AOD at 532 nm is estimated using Eq. (2) and the retrieved aerosol optical depth at 500 nm. The multiple scattering factor η will be set to 1 to agree with the CALIOP version 3 aerosol retrievals. The final lidar ratios reported by CALIOP are subsequently compared to the estimates of S_{AC} calculated in this manner in order to determine the performance of aerosol type classification and lidar ratio selection in the Brazilian territory.

4 Results

The challenge in implementing this validation methodology is to establish rigorous criteria for selecting the coincident observations between CALIOP and the ground-based systems that satisfy an optimal spatial-temporal matching window, while simultaneously obtaining a sample size sufficient to yield consistent and statistically significant results. In this section we briefly examine the trade-offs made to maximize our validation sample size, and then compare the extinction-to-backscatter ratios assigned by CALIOP aerosol subtyping system to those retrieved using the AERONET/CALIOP technique (AC technique) and to the lidar ratios retrieved from the MSP-Lidar system.

AMTD
6, 1143–1199, 2013

4.1 Data selection method

We initially determined all the CALIPSO overpasses lying within a horizontal distance of 55 km or less from the five AERONET sites. Subsequent application of the COVER-LAI/MCSA algorithm yielded 161 daytime CALIPSO measurements suitable for comparison to the sun photometer AOD data. One consequence of this filtering scheme was to entirely eliminate data three of the sites (AF, CB, and SP). The second step was to constrain the coincident measurements to fall within a temporal window up to 6 h from the time of the satellite's closest approach. Doing so further reduced the sample size to a total of 85 correlative daytime measurements, as shown in Table 3. Because the spatial constraint of $\Delta D \leq 55$ km contributed to such a large decrease the number of coincident samples, we chose to increase the horizontal distance range to $\Delta D \leq 100$ km, which still satisfies the acceptable correlation distance developed by Anderson et al. (2003). As a result, the CALIPSO and AERONET measurement coincidences increase from 85 to 237 days, as shown in Table 4, corresponding to a gain of about 179 %. For unknown reasons some data are not available in the CALIPSO subset pool and thus the initial 237 merged measurements were ultimately limited to a total of 210 measurements.

4.2 Cloud-free conditions for aerosol layers and air masses trajectories

As explained above, the backscatter centroids of the selected aerosol layers were used to initiate HYSPLIT air mass trajectories that would indicate when the air masses measured by CALIOP were measured at the AERONET sites. Figure 3 shows the HYSPLIT air mass trajectories plotted for 14 July 2009 at the Alta Floresta AERONET site. In this plot one can see the backward trajectories (in red) which were initiated at the CALIPSO footprint coordinates at 17:41 UTC (i.e. the time of the CALIPSO's closest approach). According to the trajectory time histories, the aerosol parcels measured by the AERONET sun photometer at ~ 15:00 UTC were transported to the CALIOP overpass region a bit under 3 h later (i.e. at about 17:41 UTC). In this case, the AERONET

AMTD
6, 1143–1199, 2013

AOD ($\tau_{aeronet}$) applied in Eq. (16) is the AOD retrieved by the sun photometer around 15:00 UTC. Figure 4 shows the HYSPLIT air mass forward trajectories plotted for 26 May 2007 at the São Paulo AERONET site. The forward trajectories are plotted starting at 17:00 UTC (i.e. around the time of the closest approach of the CALIPSO satellite at 17:08 UTC). The air mass parcels are transported towards the São Paulo AERONET, site arriving at ~ 20:00 UTC. Once again, the AOD used in Eq. (16) is the AOD retrieved at by the AERONET measurement closest to 20:00 UTC. Such a rigorous selection procedure considerably decreases the correlative measurements dataset, although it increases the probability that both satellite and ground-based systems are measuring the same aerosol parcels, thus increasing the reliability of the comparisons. In total, this trajectory-based validation procedure identified a merged dataset of 75 days having correlative measurements that met the criteria for the comparison of aerosol optical properties. This final dataset corresponds to about 32 % of the initial pool of coincident measurements acquired during the daytime for horizontal distances less than or equal to 100 km, as shown in Table 5.

4.3 Lidar Ratio from AERONET/CALIOP method

In the initial steps of our comparison we calculated γ'_{caliop} for all aerosol layers detected in each 20 consecutive 5-km horizontal resolution profiles, represented by red spheres at the beginning of the trajectories shown in Figs. 3 and 4. After determining the air mass arrival time at the AERONET site, we then applied equations 2 and 3 to the AERONET AOD values for 440 nm and 675 nm to derive estimates of τ^{aer}_{532}. These two quantities, γ'_{caliop} and τ^{aer}_{532} were retrieved by CALIOP and an AERONET sun photometer, respectively. From each pair of values we calculated revised lidar ratio estimates, S_{AC}, by applying the relation presented in Eq. (16). Figure 5 compares the probability distribution functions for S_{AC} to the final lidar ratios reported in the CALIPSO aerosol data products. In Fig. 5, the CALIOP final lidar ratio distribution shows a high frequency of fixed lidar ratio values at 20 sr (clean marine aerosol type), 35 sr (clean continental), 40 sr (dust), 55 sr (polluted dust) and 70 sr (smoke and polluted continental). Other

AMTD
6, 1143–1199, 2013

CALIOP values occur when the initial lidar ratio is too large, and must be lowered in order to obtain a physically meaningful extinction solution (Young and Vaughan, 2009). These results are expected, since the CALIOP retrieval algorithms use only a small set of fixed lidar ratio values. On the other hand, the lidar ratio values retrieved by the AC method show a continuous distribution spanning all of the CALIOP values. Peaks in the S_{AC} distributions can be seen around 35, 45, 55, 65 and 70 sr. Because the CALIOP model values include uncertainties that range between 35 % and 50 %, depending on aerosol type, we consider the trends in S_{AC} values to be roughly consistent with the lidar ratio models developed for the CALIOP algorithm. The mean percentage difference (MPD) between the CALIOP model and AC retrieved lidar ratios is $-8\% \pm 64\%$, calculated using the follow relation:

$$\mathrm{MPD} = \frac{S_{\mathrm{caliop}} - S_{\mathrm{AC}}}{S_{\mathrm{AC}}} \,[\%] \tag{17}$$

The high value of the standard deviation is indicative of the large dispersion in the retrieved lidar ratios. In some cases these disagreements can be a consequence of the atmospheric variability during the time of the CALIPSO closest approach and the time period which the air masses were transported to the AERONET station region. It is also important to note that this is a one-to-many analysis; that is, a single value of τ_{aeronet} was used to derive SAC for each of 20 consecutive 5-km resolution aerosol profiles (i.e. Eq. 16), as shown in Figs. 3 and 4. Doing this leaves open the possibility that in some cases the two sensors are not measuring the same air mass parcels, as can be seen by the ends of the backward trajectories in the same figures. Furthermore, it can introduce some uncertainties in those cases when a two or more aerosol types are present in the profiles. However, when calculating mean percentage differences according to CALIOP aerosol type (see Table 1), the agreement between CALIOP and the AC method is improved. The mean lidar ratio difference is $-4.5\% \pm 28\%$ for clean continental aerosol type, $-7.4\% \pm 41\%$ for dust, $-9.6\% \pm 38\%$ for polluted dust, $9\% \pm 33\%$ for polluted continental, $20\% \pm 34\%$ for smoke, and $-15\% \pm 33\%$ for clean

AMTD
6, 1143–1199, 2013

marine aerosol type, as can be seen in Table 6. All of these mean percentage differences fall within two standard deviations of the CALIOP modeled lidar ratio. The same approach described previously was used to calculate the values of S_{AC} for the single "best matching" 5-km resolution profile. These values were then compared on a one-to-one basis to the lidar ratios assigned by the CALIOP algorithm. This analysis used only those CALIOP profiles connected directly to the AERONET sites by the air masses trajectories obtained from the HYSPLIT model, thus ensuring the greatest probability that both systems have measured the same aerosol parcels. The best matching profiles in Figs. 3 and 4 are designated with a star character (★). Figure 6 shows the lidar ratio probability distribution functions for the S_{AC} and the CALIOP aerosol model value for the best matching profiles for each day of correlative measurements. As it the previous analysis, the CALIOP data shows high frequencies of fixed lidar ratio values at 35, 40, 55 and 70 sr. Similarly, the S_{AC} retrieval once again shows a broader distribution that spans all of the CALIOP lidar ratios, with some predominant peaks for dust, around 40 sr, polluted dust aerosol, around 55 sr, and biomass burning or polluted continental aerosol, around 70 sr. The lidar ratio distribution for the best matching profiles yields a mean percentage difference between S_{AC} and the CALIOP modeled value of of $-2\% \pm 26\%$. In this case, for the best matching profiles, the mean percentage difference between CALIOP and AC method lidar ratios separated according to aerosol type is $-8.6\% \pm 8.1\%$ for clean continental aerosol type, $-7\% \pm 11\%$ for dust, $-5\% \pm 13\%$ for polluted dust, $2\% \pm 14\%$ for polluted continental, and $2.9\% \pm 24\%$ for smoke aerosol type, as can be seen in Table 7. When the lidar ratios are separated according to the modeled CALIOP aerosol types, all percentage differences fall within one standard deviation of the CALIOP model, as shown in Fig. 7.

4.4 Lidar ratio from MSP-Lidar

In this section we present comparisons between the CALIOP lidar ratios and those retrieved with the MSP elastic backscatter lidar system in São Paulo (Landulfo et al., 2003, 2005). Comparisons are restricted to those days when the CALIOP point of

AMTD
6, 1143–1199, 2013

closest approach was located within less than 100 km from the MSP-Lidar site. In addition, we require that the measurements made by CALIOP, the MSP-Lidar and the AERONET sun photometer all be cloud-free, thus satisfying all the validation criteria described in Sect. 3. CALIOP lidar ratios for the 20 consecutive 5-km profiles centered at the closest distance between the CALIOP ground-track and the MSP-Lidar site were retrieved. However, for this comparison we once again used only the best matching profile (i.e. as in Sect. 4.3). The CALIOP model lidar ratios were then compared with the lidar ratios retrieved from the combination of MSP-Lidar and sun photometer measurements. Table 8 presents the lidar ratios from CALIOP and the MSP-Lidar, the percentage difference for each day analyzed, and the horizontal distance between the two measurements. In the Metropolitan Area of São Paulo (MASP), which is a region loaded by different types of aerosols generated by several sources, the CALIOP algorithm selected lidar ratios that ranged from 55 to 70 sr, representing polluted dust, continental polluted and smoke (biomass burning) aerosol types. Table 8 shows that the values obtained by both systems are very similar, though in some cases the CALIOP lidar ratio seems to be lower, probably due to the large variability of the aerosol loading in the MASP and the fairly large distance between the two sets of measurements. Nevertheless, comparison with CALIOP final lidar ratio yields a mean percentage difference of $-2\% \pm 15\%$.

4.5 Lidar Ratio retrieved from AERONET data

To further assess the significance of the lidar ratio biases obtained using the AC method (Sect. 4.3) and the CALIOP/MSP-Lidar comparison (Sect. 4.4), we used Eq. (4) to calculate LR values using inversion data from the AERONET retrievals, and then compared the results with the values assigned by the CALIOP algorithm. From a total of 75 correlative measurements between AERONET and CALIOP, there were 48 cases for which AERONET reported single-scattering albedo and 180° phase function products (here we consider Level 1.5 and Level 2 AERONET data). Good agreement between CALIOP and the AERONET retrievals is found at the Alta Floresta site, where

AMTD
6, 1143–1199, 2013

the mean lidar ratio difference is 0.2% ± 27%. For the Campo Grande site the difference rises to 3.1% ± 5.7%, representing a small overestimate by the CALIOP model values. For Cuiabá and Rio Branco the mean differences are −5.9% ± 30.7% and −4.4% ± 9.6%, respectively, while for São Paulo a larger bias of −14.4% ± 17.7% is found. In general, the comparison between both systems indicates a relatively small underestimation of the LR assigned by the CALIOP scheme, with an overall mean percentage difference of −3.9% ± 22.3% being derived from all 48 correlative measurements. Since the AERONET Level 1.5 data are pre-calibrated and cloud-screened but not post-calibrated, it is more reliable to use only the Level 2 data (Holben et al., 1998). Few Level 2 data with single-scattering albedo and 180° phase function products were available for these cases. Restricting the analysis to Level 2 data, only 9 level 2 correlative measurements are available, from which we obtained a mean difference of −2.5% ± 10.6%, indicating that the CALIOP assignments slightly underestimate the ground-based retrievals.

5 Discussion and conclusions

In this first quantitative assessment of the performance of the CALIOP lidar ratio selection algorithm over South America, lidar ratio values were calculated using Eq. (16) for 75 cloud-free coincident measurements of CALIOP and the AERONET sun photometers. A mean percentage difference of −8% ± 64% was obtained by comparing the lidar ratios from the AC calculation with those reported in CALIOP's 20 consecutive 5-km horizontal resolution profiles. When we used only the best matching profiles indicated by HYSPLIT backward or forward trajectories the percentage difference decreased to −2%±26%. Comparing these results shows that using model trajectories to correlate measurements between instruments separated spatially and temporally can considerably improve the correspondence between the two separate estimates of the same parameter. This improvement occurs precisely because our validation technique greatly increases the likelihood that the same air mass is probed by both the ground

AMTD
6, 1143–1199, 2013

and satellite based systems. The comparison of lidar ratios retrieved by the MSP-Lidar and selected by the CALIOP algorithm also shows good agreement, with a mean percentage difference of $-2\% \pm 15\%$ for the best matching profiles. Finally, comparisons between lidar ratios retrieved from AERONET sun photometer data alone were compared with the model values assigned by the CALIOP algorithm, and the mean percentage difference is also small, at $-2.5\% \pm 11\%$. These results show a strong indication that the lidar ratio values used a priori in the CALIOP algorithms are well suited to the aerosol distributions measured by ground-based systems in Brazilian territory. Our comparison methodology was developed with the aim of being the first CALIPSO validation study in the SAA region. We expect that this effort will be useful for further aerosol studies in the region and for additional validation of the CALIOP spaceborne lidar, as this location presents a significant challenge to the performance of CALIOP's calibration, layer detection and layer type identification processes, since the SAA noise induced signal can introduce significant errors in the calculation of the calibration coefficients (Powell et al., 2009). It is also important to note that random and systematic uncertainties certainly are present in this methodology. One cannot discount effects that can be related to errors in molecular and aerosol backscatter assumptions in the calibration processes of the MSP-lidar and AERONET sun photometer systems. However this first validation study in SAA region presents consistent results using different approaches, and it is also consistent with previous studies developed in other regions of the globe using instruments and techniques slightly different from those employed in this study.

In regard to other validation studies, we highlight those conducted under the aegis of EARLINET (Matthais et al., 2009). Mamouri et al. (2009) used a Raman lidar and an elastic backscatter lidar system, for nighttime and daytime, respectively, in order to develop a validation process of the CALIOP 532 nm total attenuated backscatter profile. This study analyzed 40 coincident measurements within a maximum distance of 100 km between the CALIOP overpasses and ground-based lidar system. These comparisons yielded a mean bias of $-7\% \pm 6\%$ for the total attenuated backscatter profiles

AMTD
6, 1143–1199, 2013

for altitudes between 3 and 10 km during clear sky conditions. The better agreement was found during the nighttime measurements, at −4 % ± 6 % versus −10 % ± 12 % for daytime. However, for the vertical range of 1–3 km the biases were much larger, −15 % ± 16 % and −34 % ± 34 % for nighttime and daytime, respectively. This was attributed to the increased horizontal aerosol inhomogeneity in the Planetary Boundary Layer (PBL) region, and suggests that the PBL is ill-suited for the application of traditional validation techniques that are restricted to spatial and temporal matching only. Mona et al. (2009) analyzed a total of 68 coincident measurements of level 1-version 2.01 of CALIOP 532 nm attenuated backscatter profiles using a multi-wavelength Raman lidar system. From all these cases, 16 nighttime measurements showed a good agreement between the observations of both systems with some differences especially in the boundary layer region and at high altitudes due the presence of cirrus clouds. Analysis of 11 cases with very clear atmospheric conditions showed mean percentage differences of −2 % ± 12 % between 3 km and 8 km and −24 % ± 20 % in the PBL, thus offering further evidence that spatial and temporal matching alone are insufficient for PBL validation. Pappalardo et al. (2010) report a mean relative difference of 4.6 % ± 50 % (CALIOP higher) in the altitude range of 1–10 km when comparing the 532 nm attenuated backscatter profiles of the CALIOP systems and several EARLINET lidar instruments. Such studies suggest that differences in the viewing geometries (i.e. uplooking vs. downlooking) and spatial and temporal mismatches between CALIOP and the ground-based Raman lidars, which exacerbate the influences of local sources of aerosol and complex terrain between satellite track and ground station, may lead to ambiguous results in the validation comparisons.

Perhaps the most accurate CALIOP validation to date is the comprehensive evaluation conducted by Rogers et al. (2011), which uses the LaRC HSRL aboard an aircraft underflying the trajectory of CALIPSO satellite to assess the CALIOP 532 nm attenuated backscatter profile calibration. This study examines 86 HSRL validation flights of the CALIPSO satellite during both nighttime and daytime in several regions of North America. Comparisons between CALIOP's 532 nm version 3 attenuated

AMTD
6, 1143–1199, 2013

backscatter product with HSRL attenuated backscatter profiles found a mean difference of 2.7 % ± 2.1 % (CALIOP lower) and 2.9 % ± 3.9 % (CALIOP lower), for nighttime and daytime measurements, respectively, including comparisons inside the PBL. While the previous EARLINET studies suggest that CALIOP may be biased low in the PBL, the spatially matched measurements of Rogers et al. (2011) show excellent agreement between the HSRL and CALIOP measurements in this region. When CALIOP data is compared to coincident downlooking HSRL lidar measurements the PBL variability presented in EARLINET's up-looking comparisons are not detected. Table 9 summarizes some CALIOP validation results obtained by other quantitative studies. These earlier validation studies indicate that CALIOP is well calibrated in the free troposphere region (Mona et al., 2009; Mamouri et al., 2009; Pappalardo et al., 2010). However, results obtained in such studies also point to large differences in comparisons within the PBL region, showing how rapidly the air masses in this region can change. These changes highlight the importance of employing air mass trajectories in order to reduce the uncertainties in validation comparisons and constrain measurements separated in space and time.

As was the case for the EARLINET studies, the data selected for this validation study was confined almost entirely to the PBL, and the air mass trajectory technique was applied specifically in hopes of avoiding the large discrepancies encountered by the EARLINET researchers. As shown in Sect. 4.3, the use of a single AOD value measured in a single position at the AERONET site and applied to the CALIOP's 5-km resolution aerosol profiles results in good agreement between the AC method and the CALIOP modeled lidar ratio. In our initial analysis, applying a single AERONET AOD to 20 consecutive 5-km resolution CALIOP profiles produced a mean fractional difference of −8 % ± 64 % in lidar ratio. The large spread in the results suggests that in some cases the AOD retrieved by the AERONET system applied to the Eq. (16) may not be the most appropriate value, which in turn suggests that the aerosol loading may not be sufficiently homogenous along a 100-km CALIOP ground track. When the same approach is applied to the single CALIOP 5-km profile that is most directly linked to the

AMTD
6, 1143–1199, 2013

AERONET site by the HYSPLIT trajectories (i.e. the best matching profile) the mean fractional difference found decreases to $-2\% \pm 26\%$, thus demonstrating the effectiveness of the trajectory scheme in reducing the variability of the validation comparisons. When CALIOP's modeled lidar ratios are separated by type, the mean percentage LR difference for each type lies within one standard deviation of the CALIOP models, which suggesting that the CALIOP aerosol typing scheme is reasonably accurate and that the CALIOP models provide a faithful representation of the aerosol types detected in Brazil. Comparisons between PBL lidar ratios assigned by CALIOP to those retrieved by MSP-Lidar found a mean fractional difference of $-2\% \pm 15\%$, which we consider to be very good agreement since the MASP's atmosphere is heavily loaded by several different types of aerosols, and thus represents an especially challenging validation scenario.

In the present study, the use of the best matching profile based on the HYSPLIT air masses trajectories analysis decreases the number of the comparisons between CALIPSO and ground-based instruments. However, the backward and forward trajectories approach proves to be essential in achieving consistent comparisons between the two data sets. Summarizing, it is important to emphasize that this first validation study of the CALIPSO satellite using two different remote sensing instruments in the South America is an initial effort to investigate the reliability of the aerosol optical properties retrieved by CALIPSO in the SSA region. Lidar ratio values assigned by CALIOP are in good agreement with those retrieved by the AC method, as well as with those retrieved using the MSP-Lidar + AERONET measurements. We therefore conclude that despite the many challenges faced by the CALIOP aerosol subtyping and lidar ratio selection algorithm, the algorithm is working well and shows good accuracy within Brazil. Furthermore, our results demonstrate that air mass trajectories provide a useful and reliable method for properly comparing boundary layer measurements made by CALIOP and ground-based systems and for better constraining measurements that can be widely separated in space and time.

Acknowledgements. The first author wishes to acknowledge the financial support of Fundação para o Amparo da Pesquisa do Estado de São Paulo – FAPESP under the project number

AMTD
6, 1143–1199, 2013

2011/14365-5, the support of Conselho Nacional de Energia Nuclear – CNEN/Brazil. The authors wish to acknowledge the entire CALIPSO team for their substantial contributions and for the data obtained from the NASA Langley Research Center. They also gratefully acknowledge the team of AERONET sun photometer network and the PI of each site (Brent Holben, Enio Pereira and Paulo Artaxo), and also the NOAA Air Resources Laboratory for providing the HYSPLIT transport and dispersion model and the READY website used in this publication.

References

Ackermann, J.: The extinction-to-backscatter ratio of tropospheric aerosol: a numerical study, J. Atmos. Ocean. Technol., 15, 1043–1050, doi:10.1175/1520-0426(1998)015<1043:TETBRO>2.0.CO;2, 1998 1153

Anderson, T. L, Charlson, R. J., Winker, D. M., Ogren, J. A., and Holmén, K.: Mesoscale variations of tropospheric aerosols, J. Atmos. Sci., 60, 119–136, doi:10.1175/1520-0469(2003)060<0119:MVOTA>2.0.CO;2, 2003. 1145, 1162, 1166

Anderson, T. L., Charlson, R. J., Bellouin, N., Boucher, O., Chin, M., Christopherand, S. A., Haywood, J., Kaufman, Y. J., Kinne, S., Ogrenand, J. A., Remer, L. A., Takemura, T., Tanré, D., Torres, O., Trepte, C. R., Wielicki, B. A., Winker, D. M., and Yu, H.: An "A-Train" strategy for quantifying direct climate forcing by anthropogenic aerosols, Bull. Am. Meteorol. Soc., 86, 1795–1809, doi:10.1175/BAMS-86-12-1795, 2005. 1145

Ångström, A.: The parameters of atmospheric turbidity, Tellus, 16, 64–75, doi:10.1111/j.2153-3490.1964.tb00144.x, 1964. 1150

Artaxo, P., Martins, J. V., Yamasoe, M. A., Procópio, A. S., Pauliquevis, T. M., Andrea, M. O., Guyon, P., Gatti, L. V., and Leal, A. M. C.: Physical and chemical properties of aerosols in the wet and dry seasons in Rondônia, Amazônia, J. Geophys. Res., 107, D208081, doi:10.1029/2001JD000666, 2002. 1161

Barnaba, F. and Gobbi, G. P.: Modeling the aerosol extinction versus backscatter relationship for Lidar applications: maritime and continental conditions, J. Atmos. Ocean. Technol., 21, 428–442, doi:10.1175/1520-0426(2004)021<0428:MTAEVB>2.0.CO;2, 2003. 1153

Bodhaine B. A., Wood, N. B., Dutton, E. G., and Slusser, J. R.: On Rayleigh optical depth calculations, J. Atmos. Ocean. Technol., 16, 1854–1861, doi:10.1175/1520-0426(1999)016<1854:ORODC>2.0.CO;2, 1999. 1155

AMTD
6, 1143–1199, 2013

Bucholtz, A.: Rayleigh-scattering calculations for the terrestrial atmosphere, Appl. Opt., 34, 2765–2773, doi:10.1364/AO.34.002765, 2009. 1155

Burton, S. P., Ferrare, R. A., Hostetler, C. A., Hair, J. W., Kittaka, C., Vaughan, M. A., Obland, M. D., Rogers, R. R., Cook, A. L., Harper, D. B., and Remer, L. A.: Using airborne high spectral resolution lidar data to evaluate combined active plus passive retrievals of aerosol extinction profiles, J. Geophys. Res., 115, D00H15, doi:10.1029/2009JD012130, 2010. 1147

Cattrall, C., Reagan, J., Thome, K., and Dubovik, O.: Variability of aerosol and spectral lidar and backscatter and extinction ratios of key aerosol types derived from selected Aerosol Robotic Network locations, J. Geophys. Res., 110, D10S11, doi:10.1029/2004JD005124, 2005. 1154

Charlson, R. J., Schwartz, S. E., Hales, J. M., Cess, R. D., Coakley, J. A., Hansen, J. E., and Hofmann, D. J.: Climate forcing by anthropogenic aerosols, Science, 225, 423–430, doi:10.1126/science.255.5043.423, 1992. 1145

Draxler, R. and Hess, G.: Description of the HYSPLIT 4 modeling system, NOAA Tech. Memo. ERL ARL-224, NOAA Air Resources Laboratory, Silver Spring, MD, USA, available at: http://ready.arl.noaa.gov/HYSPLIT.php (last access: 15 May 2011), 1998. 1163

Dubovik, O. and King, M. D.: A flexible inversion algorithm for retrieval of aerosol optical properties from sun and sky radiance measurements, J. Geophys. Res., 105, 20673–20696, doi:10.1029/2000JD900282, 2000. 1149

Dubovik, O., Smirnov, A., Holben, B. N., King, M. D., Kaufman, Y. J., Eck, T. F., and Slutsker, I.: Accuracy assessments of aerosol optical properties retrieved from AErosol RObotic Network (AERONET) sun and sky radiance measurements, J. Geophys. Res., 105, 9791–9806, doi:10.1029/2000JD900040, 2000. 1150

Garnier, A., Pelon, J., Dubuisson, P., Faivre, M., Chomette, O., Pascal, N., and Kratz, D. P.: Retrieval of cloud properties using CALIPSO Imaging Infrared Radiometer, Part I: effective emissivity and optical depth, J. Appl. Meteor. Climatol., 51, 1407–1425, doi:10.1175/JAMC-D-11-0220.1, 2012. 1156

Giannakaki, E., Balis, D. S., Amiridis, V., and Zerefos, C.: Optical properties of different aerosol types: seven years of combined Raman-elastic backscatter lidar measurements in Thessaloniki, Greece, Atmos. Meas. Tech., 3, 569–578, doi:10.5194/amt-3-569-2010, 2010. 1154

Hlavka, D., Yorks, J., Young, S., Vaughan, M., Kuehn, R., McGill, M., and Rodier, S.: Airborne validation of cirrus cloud properties derived from CALIPSO Lidar measurements: optical properties, J. Geophys. Res., 117, D09207, doi:10.1029/2011JD017053, 2012. 1147

AMTD
6, 1143–1199, 2013

Holben, B. N., Eck, T. F., Slutsker, I., Tanré, D., Buis, J. P., Setzer, A., Vermote, E., Reagan, J. A., Kaufman, Y. J., Nakajima, T., Lavenu, F., Jankowiak, I., and Smirnov, A.: Aeronet – a federal instrument network and data archive for aerosol characterization, Remote Sens. Environ., 66, 1–16, doi:10.1016/S0034-4257(98)00031-5, 1998. 1149, 1150, 1171

Hostetler, C. A., Liu, Z., Reagan, J., Vaughan, M. A., Winker, D. M., Osborn, M., Hunt, W. H., Powell, K. A., and Trepte, C.: CALIOP Algorithm Theoretical Basis Document – Calibration and level 1 data products, release 1.0, PC-SCI-201 Part 1, NASA Langley Research Center, Hampton, Virginia, USA, available at: http://www-calipso.larc.nasa.gov/resources/project_documentation.php (last access: 10 June 2010), 2006. 1156, 1158

Hu, Y., Winker, D. M., Vaughan, M. A., Lin, B., Omar, A., Trepte, C., Flittner, D., Yang, P., Nasiri, S. L., Baum, B., Holz, R., Sun, W., Liu, Z., Wang, Z., Young, S., Stamnes, K., Huang, J., and Kuehn, R.: CALIPSO/CALIOP cloud phase discrimination algorithm, J. Atmos. Ocean. Technol., 26, 2293–2309, doi:10.1175/2009JTECHA1280.1, 2009. 1159

Hunt, W. H., Winker, D. M., Vaughan, M. A., Powell, K. A., Lucker, P. L., and Weimer, C.: CALIPSO Lidar description and performance assessment, J. Atmos. Ocean. Technol., 26, 1214–1228, doi:10.1175/2009JTECHA1223.1, 2009. 1146, 1148, 1156, 1158, 1159

Kacenelenbogen, M., Vaughan, M. A., Redemann, J., Hoff, R. M., Rogers, R. R., Ferrare, R. A., Russell, P. B., Hostetler, C. A., Hair, J. W., and Holben, B. N.: An accuracy assessment of the CALIOP/CALIPSO version 2/version 3 daytime aerosol extinction product based on a detailed multi-sensor, multi-platform case study, Atmos. Chem. Phys., 11, 3981–4000, doi:10.5194/acp-11-3981-2011, 2011. 1147

Kim, S.-W., Berthier, S., Raut, J.-C., Chazette, P., Dulac, F., and Yoon, S.-C.: Validation of aerosol and cloud layer structures from the space-borne lidar CALIOP using a ground-based lidar in Seoul, Korea, Atmos. Chem. Phys., 8, 3705–3720, doi:10.5194/acp-8-3705-2008, 2008. 1146, 1160

Kittaka, C., Winker, D. M., Vaughan, M. A., Omar, A., and Remer, L. A.: Intercomparison of column aerosol optical depths from CALIPSO and MODIS-Aqua, Atmos. Meas. Tech., 4, 131–141, doi:10.5194/amt-4-131-2011, 2011. 1147

Klett, J. D.: Stable analytical inversion solution for processing lidar returns, Appl. Opt., 20, 211–220, doi:10.1364/AO.20.000211, 1981. 1154

Klett, J. D.: Lidar inversion with variable backscatter/extinction ratios, Appl. Opt., 24, 1638–1643, doi:10.1364/AO.24.001638, 1985. 1146, 1154

AMTD
6, 1143–1199, 2013

Kovacs, T.: Comparing MODIS and AERONET aerosol optical depth at varying separation distances to assess ground-based validation strategies for spaceborne Lidar, J. Geophys. Res., 111, D24203, doi:10.1029/2006JD007349, 2006. 1162

Landulfo, E., Papayannis, A., Artaxo, P., Castanho, A. D. A., de Freitas, A. Z., Souza, R. F., Vieira Junior, N. D., Jorge, M. P. M. P., Sánchez-Ccoyllo, O. R., and Moreira, D. S.: Synergetic measurements of aerosols over São Paulo, Brazil using LIDAR, sunphotometer and satellite data during the dry season, Atmos. Chem. Phys., 3, 1523–1539, doi:10.5194/acp-3-1523-2003, 2003. 1151, 1169

Landulfo, E., Papayannis, A., Artaxo, P., Castanho, A. D. A., de Freitas, A. Z., Souza, R. F., Vieira Junior, N. D., Jorge, M. P. P. M., Sánchez-Ccoyllo, O. R., and Moreira, D. S.: Tropospheric aerosol observations in São Paulo, Brazil using a compact Lidar system, Int. J. Remote Sens., 26, 2797–2816, doi:10.1080/01431160500033971, 2005. 1152, 1169

Landulfo, E., Papayannis, A., Torres, A. S., Uehara, S. T., Pozzetti, L. M. V., de Matos, C. A., Sawamura, P., Nakaema, W. M., and de Jesus, W. C.: A four-year Lidar-sun photometer aerosol study at São Paulo, Brazil, J. Atmos. Ocean. Technol., 25, 1463–1468, doi:10.1175/2007JTECHA984.1, 2008. 1162

Lee, K.-P., Vaughan, M. A., Liu, Z., Hunt, W., and Powell, K.: Revised Calibration Strategy for the CALIOP 532 nm Channel: Part 1 – Nighttime, Reviewed and Revised Papers Presented at the 24th International Laser Radar Conference, Boulder, Colorado, USA, 23–27 June, 1173–1176, 2008. 1159

Liou, K. N.: An Introduction to Atmospheric Radiation, 2nd edn., Academic Press, New York, 583 pp., 2002. 1153

Liu, Z., Vaughan, M. A., Winker, D. M., Kittaka, C., Getzewich, B. J., Kuehn, R. E., Omar, A. H., Powell, K. A., Trepte, C. R., and Hostetler, C. A.: The CALIPSO Lidar cloud and aerosol discrimination: version 2 algorithm and initial assessment of performance, J. Atmos. Ocean. Technol., 26, 1198–1213, doi:10.1175/2009JTECHA1231.1, 2009. 1159, 1163

Mamouri, R. E., Amiridis, V., Papayannis, A., Giannakaki, E., Tsaknakis, G., and Balis, D. S.: Validation of CALIPSO space-borne-derived attenuated backscatter coefficient profiles using a ground-based lidar in Athens, Greece, Atmos. Meas. Tech., 2, 513–522, doi:10.5194/amt-2-513-2009, 2009. 1146, 1160, 1172, 1174

Matthais, V., Freudenthaler, V., Amodeo, A., Balin, I., Balis, D., Bösenberg, J., Chaikovsky, A., Chourdakis, G., Comeron, A., Delaval, A., De Tomasi, F., Eixmann, R., Hågård, A., Komguem, L., Kreipl, S., Matthey, R., Rizi, V., Rodrigues, J. A., Wandinger, U., and Wang, X.:

AMTD
6, 1143–1199, 2013

Aerosol Lidar intercomparison in the framework of the EARLINET project, 1: instruments, Appl. Opt., 13, 961–976, doi:10.1364/AO.43.000961, 2004. 1172
McGill, M. J., Vaughan, M. A., Trepte, C. R., Hart, W. D., Hlavka, D. L., Winker, D. M., and Kuehn, R.: Airborne validation of spatial properties measured by the CALIPSO Lidar, J. Geophys. Res., 112, D20201, doi:10.1029/2007JD008768, 2007. 1147
McPherson, C. J., Reagan, J. A., Schafer, J., Giles, D., Ferrare, R., Hair, J., and Hostetler, C.: AERONET, airborne HSRL, and CALIPSO aerosol retrievals compared and combined: a case study, J. Geophys. Res., 115, D00H21, doi:10.1029/2009JD012389, 2010. 1147
Miranda, R. M. and Andrade, M. F.: Physicochemical characteristics of atmospheric aerosol during winter in the São Paulo metropolitan area in Brazil, Atmos. Environ., 39, 6188–6193, doi:10.1016/j.atmosenv.2005.06.055, 2005. 1162
Mona, L., Pappalardo, G., Amodeo, A., D'Amico, G., Madonna, F., Boselli, A., Giunta, A., Russo, F., and Cuomo, V.: One year of CNR-IMAA multi-wavelength Raman lidar measurements in coincidence with CALIPSO overpasses: Level 1 products comparison, Atmos. Chem. Phys., 9, 7213–7228, doi:10.5194/acp-9-7213-2009, 2009. 1146, 1155, 1160, 1173, 1174
Omar, A. H., Won, J.-G., Winker, D. M., Yoon, S.-C., Dubovik, O., and McCormick, M. P.: Development of global aerosol models using cluster analysis of Aerosol Robotic Network (AERONET) measurements, J. Geophys. Res., 110, D10S14, doi:10.1029/2004JD004874, 2005. 1159
Omar, A. H., Winker, D. M., Kittaka, C., Vaughan, M. A., Liu, Z., Hu, Y., Trepte, C. R., Rogers, R. R., Ferrare, R. A., Lee, K., Kuehn, R. E., and Hostetler, C. A.: The CALIPSO automated aerosol classification and Lidar ratio selection algorithm, J. Atmos. Ocean. Technol., 26, 1994–2014, doi:10.1175/2009JTECHA1231.1, 2009. 1151, 1159, 1160
Omar, A. H., Winker, D. M., Tackett, J., Kar, J., Liu, Z., Vaughan, M., Powell, K., and Trepte, C.: CALIPSO AERONET aerosol optical depth intercomparisons: one size fits none, J. Geophys. Res., under review, 2013. 1147, 1148
Pappalardo, G., Wandinger, U., Mona, L., Hiebsch, A., Mattis, I., Amodeo, A., Ansmann, A., Seifert, P., Linné, H., Apituley, A., Arboledas, L. A., Balis, D., Chaikovsky, A., D' Amico, G., De Tomasi, F., Freudenthaler, V., Giannakaki, E., Giunta, A., Grigorov, I., Iarlori, M., Madonna, F., Mamouri, R. E., Nasti, L., Papayannis, A., Pietruczuk, A., Pujadas, M., Rizi, V., Rocadenbosch, F., Russo, F., Schnell, F., Spinelli, N., Wang, X., and Wiegner, M.: EARLINET

AMTD
6, 1143–1199, 2013

correlative measurements for CALIPSO: first intercomparison results, J. Geophys. Res., 115, D00H19, doi:10.1029/2009JD012147, 2007. 1147, 1173, 1174

Pitts, M. C., Thomason, L. W., Hu, Y., and Winker, D. M.: An assessment of the on-orbit performance of the CALIPSO wide field camera, in: Remote Sensing of Clouds and the Atmosphere XII Proceedings of SPIE, Florence, Italy, 25 October, 675, 67450k, doi:10.1117/12.737377, 2007. 1156

Platt, C. M. R.: Lidar and radiometer observations of cirrus clouds, J. Atmos. Sci., 30, 1191–1204, doi:10.1175/1520-0469(1973)030<1191:LAROOC>2.0.CO;2, 1973. 1164

Powell, K. A., Vaughan, M. A., Kuehn, R., Hunt, W. H., and Lee, K.-P.: Revised calibration strategy for the caliop 532-nm channel: Part II daytime, Reviewed and Revised Papers Presented at the 24th International Laser Radar Conference, Boulder, Colorado, USA, 23–27 June, 1177–1180, 2008. 1158

Powell, K. A., Hostetler, C. A., Liu, Z., Vaughan, M. A., Kuehn, R. E., Hunt, W. H., Liu, K., Trepte, C. R., Rogers, R. R., Young, S. A., and Winker, D. M.: CALIPSO Lidar calibration algorithms part I: nighttime 532 nm parallel channel and 532 nm perpendicular channel, J. Atmos. Ocean. Technol., 26, 2015–2033, doi:10.1175/2009JTECHA1242.1, 2009. 1148, 1157, 1158, 1159, 1172

Powell, K. A., Vaughan, M. A., Rogers, R. R., Kuehn, R., Hunt, W. H., Lee, K.-P., and Murray, T. D.: The CALIOP 532-nm channel daytime calibration: version 3 algorithm, Reviewed and Revised Papers Presented at the 25th International Laser Radar Conference, St. Petersburg, Russia, 5–9 July, 1367–1370, 2010. 1158

Powell, K. A., Vaughan, M. A., Winker, D. M., Lee, K.-P., Pitts, M., Trepte, C., Detweiler, P., Hunt, W., Lambeth, J., Lucker, P., Murray, T., Hagolle, O., Lifermann, A., Faivre, M., Garnier, A., and Pelon, J.: CALIPSO Data Products Catalog, Release 3.4, PC-SCI-503, NASA Langley Research Center, Hampton, VA-USA, available at: http://www-calipso.larc.nasa.gov/products/CALIPSO_DPC_Rev3x4.pdf (last access: 10 June 2010), 2011. 1162

Rogers, R. R., Hostetler, C. A., Hair, J. W., Ferrare, R. A., Liu, Z., Obland, M. D., Harper, D. B., Cook, A. L., Powell, K. A., Vaughan, M. A., and Winker, D. M.: Assessment of the CALIPSO Lidar 532 nm attenuated backscatter calibration using the NASA LaRC airborne High Spectral Resolution Lidar, Atmos. Chem. Phys., 11, 1295–1311, doi:10.5194/acp-11-1295-2011, 2011. 1148, 1173, 1174

Russell, P. B., Swissler, T. J., and McCormick, M. P.: Methodology for error analysis and simulation of lidar aerosol measurements, Appl. Opt., 18, 3783–3797, 1979. 1157

AMTD
6, 1143–1199, 2013

Solomon, S., Qin, D., Manning, M., Chen, Z., Marquis, M., Averyt, K. B., Tignor, M., and Miller, H. L.: Contribution of Working Group I to the Fourth Assessment Report of the Intergovernmental Panel on Climate Change, 1st edn., Cambridge University Press, UK and New York, 996 pp., 2007. 1145

Schuster, G. L., Vaughan, M., MacDonnell, D., Su, W., Winker, D., Dubovik, O., Lapyonok, T., and Trepte, C.: Comparison of CALIPSO aerosol optical depth retrievals to AERONET measurements, and a climatology for the lidar ratio of dust, Atmos. Chem. Phys., 12, 7431–7452, doi:10.5194/acp-12-7431-2012, 2012. 1147, 1148

Stephens, G. L., Vane, D. G., Boain, R. J., Mace, G. G., Sassen, K., Wang, Z., Illingworth, A. J., O'Connor, E. J., Rossow, W. B., Durden, S. L., Miller, S. D., Austin, R. T., Benedetti, A., Mitrescu, C., and CloudSat Science Team: The CloudSat mission and the A-Train: a new dimension of space-based observations of clouds and precipitation, Bull. Am. Meteorol. Soc., 83, 1771–1790, doi:10.1175/BAMS-83-12-1771, 2002. 1155

Tao, Z., McCormick, M. P., and Wu, D.: A comparison method for spaceborne and ground-based lidar and its application to the CALIPSO lidar, Appl. Phys. B, 91, 639–644, doi:10.1007/s00340-008-3043-1, 2008. 1146

Vaughan, M. A., Winker, D. M., and Powell, K. A.: CALIOP Algorithm Theoretical Basis Document – Part 2: Feature detection and layer properties algorithms, Release 1.01, PC-SCI-202 Part 2, NASA Langley Research Center, Hampton, Virginia, USA, available at: http://www-calipso.larc.nasa.gov/resources/project_documentation.php (last access: 10 June 2010), 2006. 1163

Vaughan, M. A., Powell, K. A., Kuehn, R. E., Young, S. A., Winker, D. M., Hostetler, C. A., Hunt, W. H., Liu, Z., McGill, M. J., and Getzewich, B. J.: Fully automated detection of cloud and aerosol layers in the CALIPSO Lidar measurements, J. Atmos. Ocean. Technol., 26, 2034–2050, doi:10.1175/2009JTECHA1228.1, 2009. 1159

Vernier, J. P., Pommereau, J. P., Garnier, A., Pelon, J., Larsen, N., Nielsen, J., Christensen, T., Cairo, F., Thomason, L. W., Leblanc, T., and McDermid, I. S.: Tropical stratospheric aerosol layer from CALIPSO lidar observations, J. Geophys. Res., 114, D00H10, doi:10.1029/2009JD011946, 2009. 1157

Weisz, E., Li, J., Menzel, W. P., Heidinger, A. K., Kahn, B. H., and Liu, C. Y.: Comparison of AIRS, MODIS, CloudSat and CALIPSO cloud top height retrievals, Geophys. Res. Lett., 34, L17811, doi:10.1029/2007GL030676, 2007. 1147

AMTD
6, 1143–1199, 2013

Winker, D. M., Vaughan, M. A., Omar, A., Hu, Y., Powell, K. A., Liu, Z., Hunt, W. H., and Young, S. A.: Overview of the CALIPSO mission and CALIOP data processing algorithms, J. Atmos. Ocean. Technol., 26, 2310–2323, doi:10.1175/2009JTECHA1231.1, 2009. 1146, 1156

Winker, D. M., Pelon, J., Coakley Jr., J. A., Ackerman, S. A., Charlson, R. J., Colarco, P. R., Flamant, P., Fu, Q., Hoff, R., Kittaka, C., Kubar, T. L., LeTreut, H., McCormick, M. P., Megie, G., Poole, L., Powell, K., Trepte, C., Vaughan, M. A., and Wielicki, B. A.: The CALIPSO mission: a global 3-D view of aerosols and clouds, Bull. Am. Meteorol. Soc., 91, 1211–1229, doi:10.1175/2010BAMS3009.1, 2010. 1146

Wu, D., Wang, Z., Wang, B., Zhou, J., and Wang, Y.: CALIPSO validation using ground-based lidar in Hefei (31.9° N, 117.2° E), China, Appl. Phys. B, 102, 185–195, doi:10.1007/s00340-010-4243-z, 2011. 1146, 1160

Yorks, J., Hlavka, D., Vaughan, M., McGill, M., Hart, W., Rodier, S., and Kuehn, R.: Airborne validation of cirrus cloud properties derived from CALIPSO Lidar measurements: spatial properties, J. Geophys. Res., 116, D19207, doi:10.1029/2011JD015942, 2011. 1147

Young, S. A. and Vaughan, M. A.: The retrieval of profiles of particulate extinction from Cloud-Aerosol Lidar Infrared Pathfinder Satellite Observations (CALIPSO) data: algorithm description, J. Atmos. Ocean. Technol., 26, 1105–1119, doi:10.1175/2008JTECHA1221.1, 2009. 1154, 1168

AMTD
6, 1143–1199, 2013

Table 1. CALIPSO aerosol types and their associated 532 nm lidar ratio distributions.

Aerosol type	Lidar ratio
Dust	40 ± 20 sr
Smoke	70 ± 28 sr
Clean Continental	35 ± 16 sr
Polluted Continental	70 ± 25 sr
Polluted Dust	55 ± 22 sr
Clean Marine	20 ± 6 sr

AMTD
6, 1143–1199, 2013

Table 2. Geographical coordinates of the five measurement sites used in this study.

Location	Latitude	Longitude
Rio Branco (RB)	9°57′25″ S	67°52′08″ W
Alta Floresta (AF)	9°52′15″ S	56°06′14″ W
Cuiabá (CB)	15°43′44″ S	56°01′15″ W
Campo Grande (CG)	20°26′16″ S	54°32′16″ W
São Paulo (SP)	23°33′38″ S	46°44′23″ W

AMTD
6, 1143–1199, 2013

Table 3. AERONET correlative measurement days for CALIOP closest approach distances less than 55 km.

Station/Year	2006	2007	2008	2009	Total
RB	11	09	08	17	45
AF	0	0	0	0	0
CB	0	0	0	0	0
CG	0	10	15	15	40
SP	0	0	0	0	0
Total	11	19	23	32	85

AMTD
6, 1143–1199, 2013

Table 4. AERONET correlative measurement days for CALIOP closest approach distances less than 100 km.

Station/Year	2006	2007	2008	2009	Total
RB	11	09	08	17	45
AF	13	19	17	37	86
CB	13	14	13	05	45
CG	0	10	15	15	40
SP*	1	15	03	02	21
Total	38	67	56	76	237

* The correlative days for SP site refers to the AERONET sun photometer, CALIOP and MSP-Lidar system measurements.

AMTD
6, 1143–1199, 2013

Table 5. Percentage of correlative measurements under free-cloud conditions selected for application of the AC method and subsequent comparison to the optical properties retrieved by CALIOP and the AERONET sun photometers.

AERONET Station	Selected days	Total correlative measurements	Percentage
RB	45	16	35.5 %
AF	86	24	27.9 %
CB	45	12	26.6 %
CG	40	8	20 %
SP	21	15	71.4 %
Total	237	75	32 %

AMTD
6, 1143–1199, 2013

Table 6. Mean percentage lidar ratio difference between the S_{AC} calculation and the CALIOP modeled value for each twenty-consecutive 5-km horizontal resolution profiles.

Aerosol type	Mean percentage difference
Dust	−7.4 % ± 41 %
Smoke	20 % ± 34 %
Clean Continental	−4.5 % ± 28 %
Polluted Continental	9 % ± 33 %
Polluted Dust	−9.6 % ± 38 %
Clean Marine	−15 % ± 33 %

AMTD
6, 1143–1199, 2013

Table 7. Mean percentage lidar ratio difference between the S_{AC} calculation and the CALIOP modeled value for the single best matching 5-km horizontal resolution profile.

Aerosol type	Mean percentage difference
Dust	−7.0 % ± 11 %
Smoke	2.9 % ± 24 %
Clean Continental	−8.6 % ± 8.1 %
Polluted Continental	2 % ± 14 %
Polluted Dust	−5.0 % ± 13 %

AMTD
6, 1143–1199, 2013

Table 8. Summary of the comparison for the lidar ratios retrieved from CALIOP and MSP-Lidar system.

S_{CALIOP}	$S_{MSP\text{-}Lidar}$	Percentage	ΔD (km)
55	50	10.0 %	72
70	65	7.69 %	82
70	65	7.69 %	72
55	72	−23.61 %	82
55	65	−15.38 %	84
55	52	5.76 %	83
40	58	−31.03 %	79
55	55	0 %	75
55	55	0 %	80
55	50	10 %	75
55	51	7.84 %	85

AMTD
6, 1143–1199, 2013

Table 9. Summary of CALIOP validation results from previous studies.

Study	Percentage difference	Data level	Instrument employed
Rogers et al. (2011)	2.9% ± 3.9% 2.7% ± 2.1% CALIOP lower	Level 1–532 nm Total attenuated backcatter	NASA LaRC airborne HSRL system
Kacenelenbogen et al. (2011)	−52.2% (MODIS) −44.8% (POLDER) −38.4% (HSRL) −43.8% (AERONET)	Aerosol extinction Level 2 product	MODIS POLDER, NASA LaRC airborne HSRL,AERONET
Pappalardo et al. (2010)	4.6% ± 50%	Level 1–532 nm Total attenuated backcatter	Multi- wavelength lidar systems
Mona et al. (2009)	−24% ± 20% −2% ± 12%	Level 1–532 nm Total attenuated backcatter	Raman lidar systems
Mamouri et al. (2009)	−15% ± 16% −4% ± 6%	Level 1–532 nm Total attenuated backcatter	Raman lidar systems
This study	−2% ± 26% −2.5% ± 22% −2% ± 15%	Level 2 532 nm lidar ratio	AERONET and 532 nm elastic lidar

AMTD
6, 1143–1199, 2013

Fig. 1. Map of Brazil showing the five sites used in this validation study. The Rio Branco site (RB) is located in the North region of Brazil and Alta Floresta (AF), Cuiabá (CB) e Campo Grande (CG) are located in the Midwest region. The primary vegetation in all four of these regions is either savannah or rainforest, and can thus be considered as sources of biomass burning aerosol. São Paulo (SP) is located in the Southeast region of Brazil, which is heavily industrialized, and whose atmosphere can contain many different types of aerosols.

AMTD
6, 1143–1199, 2013

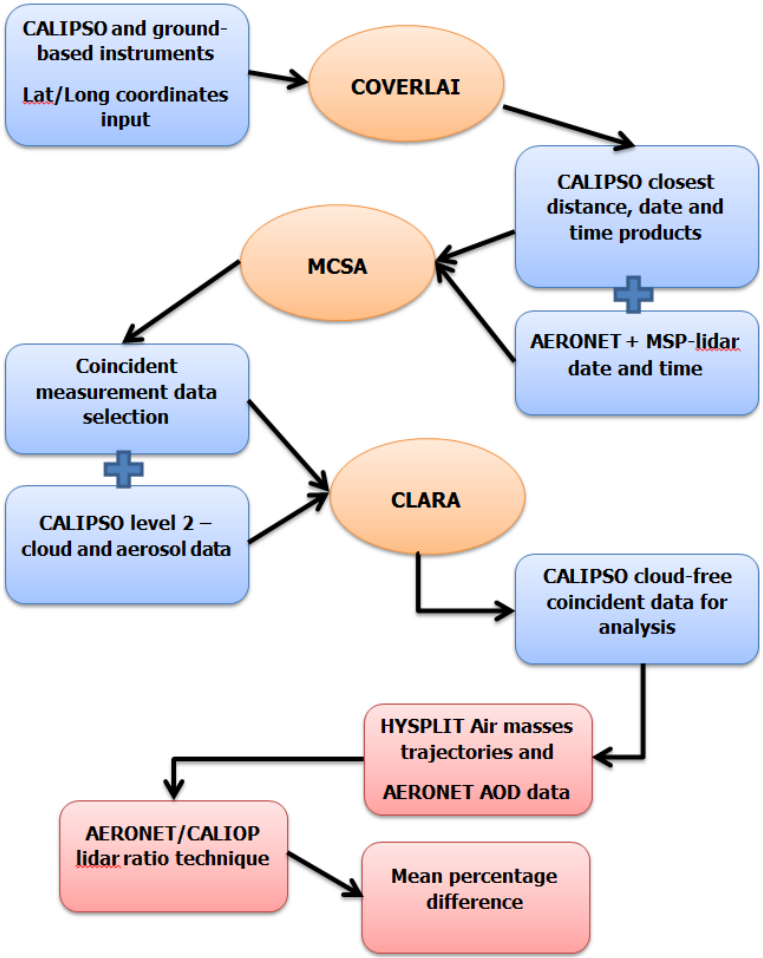

Fig. 2. Flowchart of the validation methodology and their output products.

AMTD
6, 1143–1199, 2013

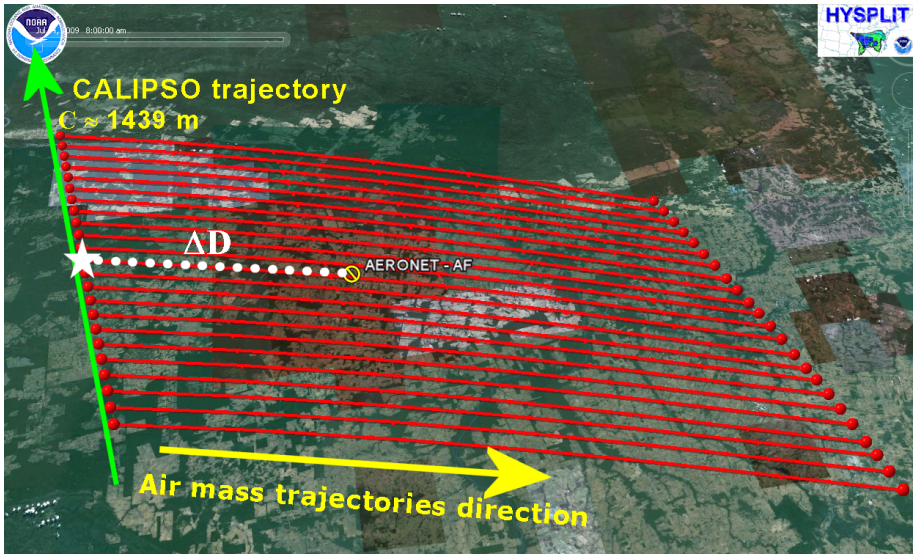

Fig. 3. HYSPLIT backward trajectories in the region of the Alta Floresta AERONET site for 14 July 2009. The backward trajectories start around the time of the CALIPSO's closest approach, at 17:41 UTC. ΔD is the closest distance between CALIPSO trajectory and the AERONET site, in this case 67.3 km. The initial lat/long coordinates have been used as the central values of lat/long for each 5-km horizontal resolution aerosol-layer profiles. The initial altitude for each trajectory, i.e. the backscatter centroids, was in this case 1439 m.

AMTD
6, 1143–1199, 2013

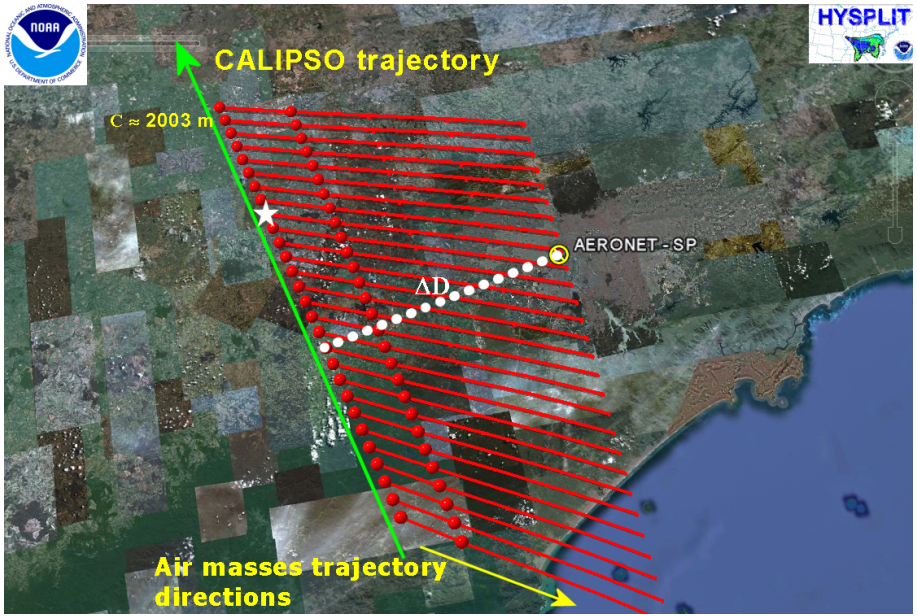

Fig. 4. HYSPLIT backward trajectories in the region of the São Paulo AERONET site for 26 May 2007. The forward trajectories start around the time of the CALIPSO's closest approach (17:08 UTC). ΔD is the closest distance between CALIPSO trajectory and the AERONET site, in this case 71.7 km. The initial lat/lon coordinates have been used as the central values of lat/lon for each 5-km horizontal resolution aerosol-layer profiles. The initial altitude for the trajectories, i.e. the backscatter centroids, was in this case about 2003 m.

AMTD
6, 1143–1199, 2013

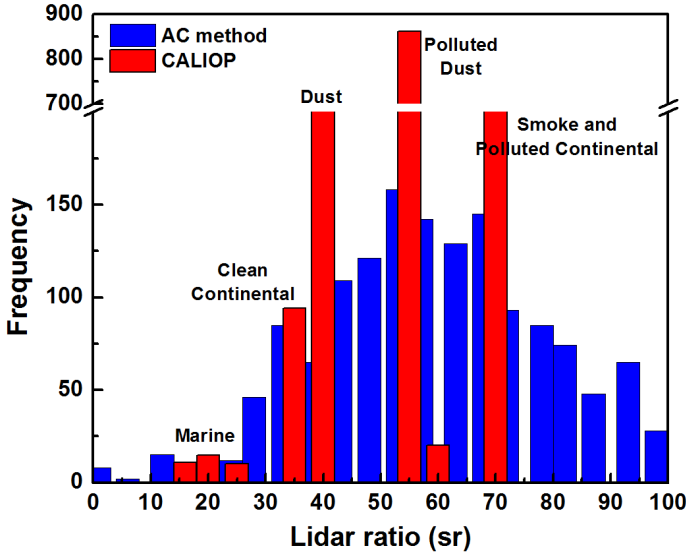

Fig. 5. Lidar ratio occurrence frequencies reported in the CALIPSO data products (red) and those derived using the AC method (blue).

AMTD
6, 1143–1199, 2013

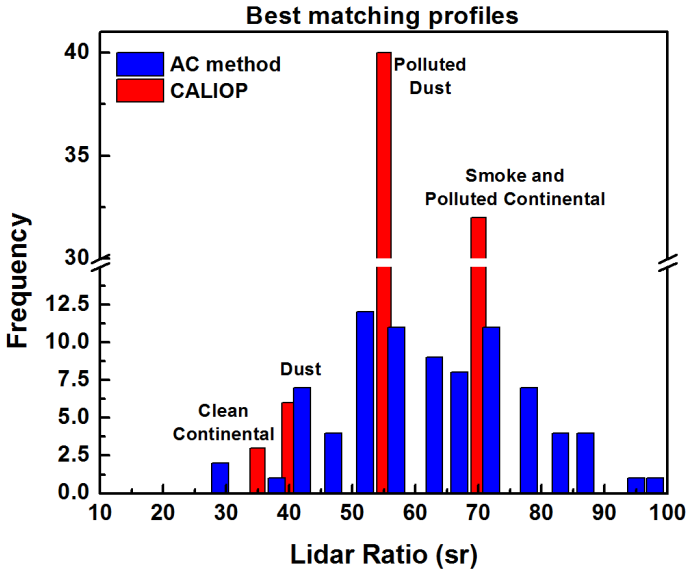

Fig. 6. Lidar ratio occurrence frequencies for CALIOP and the AC method for the best matching profile of each measurement day.

AMTD
6, 1143–1199, 2013

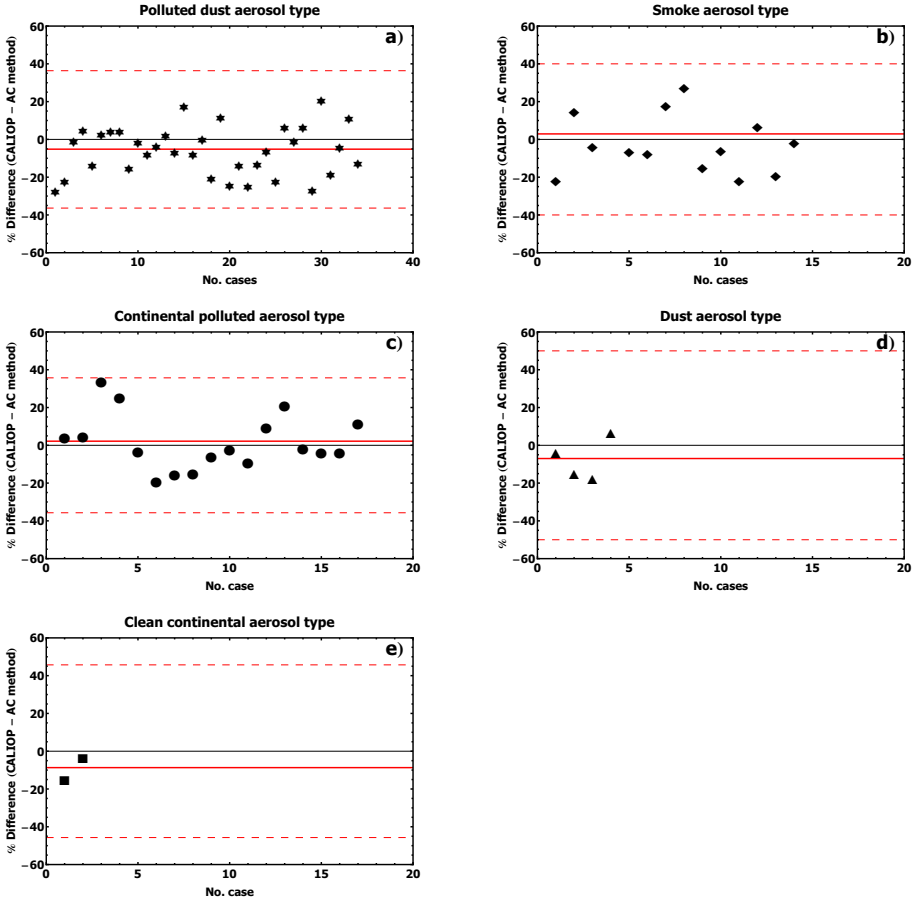

Fig. 7. Lidar ratio mean percentage difference from CALIOP and the AC technique separated according to CALIOP aerosol type and using only the best matching profiles approach. The red dashed lines represent one modeled standard deviation, and the red solid line represents the mean percentage difference values (Eq. 17) for each case.

AMTD
6, 1143–1199, 2013

Assessment of the CALIPSO Lidar 532 nm version 3 lidar ratio models

F. J. S. Lopes et al.